Chemie der Erde 78 (2018) 323–339

Contents lists available at ScienceDirect

Chemie der Erde

journal homepage: www.elsevier.com/locate/chemer

Mineralogical and geochemical implications of weathering rates in coastal dunes and beach sands close to a volcanic rock source in the western Gulf of Mexico, Mexico

Mendieta-Lora M.[a], Mejía-Ledezma R.O.[a], Kasper-Zubillaga J.J.[b,*], Arellano-Torres E.[c], Álvarez Sánchez L.F.[d]

[a] Universidad Autónoma del Estado de Hidalgo, Ingeniería en Geología Ambiental, Carretera Pachuca-Actopan Km. 4.5, Campo de Tiro, 42039, Pachuca de Soto, Hgo, México
[b] Instituto de Ciencias del Mar y Limnología, Unidad Académica de Procesos Oceánicos y Costeros, UNAM, Ciudad Universitaria s/n, 04510, CDMX, México
[c] Facultad de Ciencias, Departamento de Ecología y Recursos Naturales, UNAM Ciudad Universitaria s/n, 04510, CDMX, México
[d] Instituto de Ciencias del Mar y Limnología, Unidad de Informática Marina UNAM, Ciudad Universitaria s/n, 04510, CDMX, México

ARTICLE INFO

Handling Editor: P. D. Roy

Keywords:
Coastal dune
Beach
Mineralogy
Chemical weathering
Volcanic rocks

ABSTRACT

Coastal dune (CD) and beach sand samples were mineralogically and chemically studied to assess the weathering rates in a coastal area surrounded by the Trans-Mexican Volcanic Belt (TMVB). The study area is a narrow coastal plain with sub-humid warm weather and vigorous coastal dynamics located in the Western Gulf of Mexico (WGM). Our results show that the grain size parameters remain homogeneous along nine CD and beach sites, probably due to the hydrodynamic mechanisms prevailing in the area, i.e. wind deflation, longshore currents, and waves. The minerals found in the CD and beach sands are enriched in recycled, highly corroded monocrystalline quartz (Qm), with loss of plagioclase (P) and olivine (ol), with ilmenite fractions (op) especially in the northern sites. The geochemical data show that the sands are controlled by the exhumation of the TMVB rocks composed of a high volcanic lithic content with lathwork, microlithic, and negligible vitric textures. These volcanic fractions are in agreement with the presence of lavas of calc alkaline, andesite, Na-alkaline lavas, and rhyolite tuffs derived from the TMVB. Significant Spearman Rank Correlations (SRCs) resulted from high silica, titanium, iron, magnesium, calcium, vanadium, chromium, cobalt, associated with the presence of Qm, ilmenite, clinopyroxene, shell fragments, and volcanic lithics. Monocrystalline quartz enrichments, compared to a quartz dilution effect (< Qm; < Qm) at the northern and southern beach sites, reflect the vigorous coastal dynamics. The presence of ilmenite lag deposits in the northern sites indicate that high energy hydrodynamic conditions prevail at the site. The rare earth element (REE) patterns support the mineralogical and compositional framework of the CD and beach sands as part of the TMVB exhumation. We used various chemical indices such as the Chemical Index of Alteration (CIA), the Chemical Index of Weathering (CIW), the Plagioclase Index of Alteration (PIA), and the Weathering Index of Plagioclase (WIP). The WIP values reflect the depletion of mobile elements such as Ca, Na, K, and enrichment of Qm at the northern beach sites, e.g. the Istirinchiá site. The CIA/WIP ratio of 2.13 indicates intermediate weathering under warm climatic conditions and recycling of CD and beach sands.

1. Introduction

Chemical weathering rates have proven to be a useful quantitative approach for discussion of the associations among climate, relief, and coastal dynamics controlling the composition of old and modern continental and coastal sediments with different parent rocks (Honda and Shimizu, 1998; Dott, 2003; Garzanti et al., 2015; Muhs, 2017). In warm and humid regions, few studies have considered the mineralogical composition and weathering rates in coastal basins close to volcanic rock exposures (Marsaglia, 1993; Kasper-Zubillaga et al., 2007; Garzanti et al., 2013a, 2013b; Alappat et al., 2016). In the WGM, the CD and beach sands should reflect a compositional similarity to the TMVB, due to the proximity of the volcanic rocks to the coastal plain. However, it is unknown how the recycling, abrasion, and chemical loss of the sands' main components are controlled by climate and hydrodynamic conditions. In this study, we aimed to resolve the exogenous processes

* Corresponding author.
E-mail address: kasper@cmarl.unam.mx (J.J. Kasper-Zubillaga).

https://doi.org/10.1016/j.chemer.2018.06.004
Received 26 March 2018; Received in revised form 26 May 2018; Accepted 26 June 2018

induced by various mechanisms that can modify the sand composition (Arth, 1981). We propose the use of the CIA, CIW, PIA, and WIP to measure and determine the role of weathering conditions in the minerals (Parker, 1970; Nesbitt and Young, 1982; Fedo et al., 1995; Price and Velbel, 2003; Fiantis et al., 2010; Garzanti et al., 2013a, 2013b). Our paper contributes to the establishment of the mineralogical framework and weathering rates in a confined sedimentary basin surrounded by the TMVB under warm and humid climate (Cantagrel and Robin, 1979; Negendank et al., 1985; Gómez-Tuena et al., 2007; Ferrari et al., 2011).

2. Study area

The study area is located in the WGM (between 20°12´ and 19°24´N; 96°45´and 96°19´W). The area is part of a physiographic region described as part of the Gulf of Mexico Coastal Plain (Tamayo, 2013). Climate and chemical weathering processes affecting the coastal area are determined by the sub-humid warm weather conditions with a summer rainfall regime in a tropical geographic setting; i.e. Am (warm-humid with maxima summer rainfall), Aw (sub-humid with summer rainfall) (Kottek et al., 2006). Hurricanes are common from June to November (Tamayo, 2013). Minimum temperatures are 17–25 °C and maximum temperatures are 22–30 °C, while average precipitation ranges from 370 mm to 60 mm in summer and winter, respectively. The annual average humidity is about 80% (https://weather-and-climate.com).

Coastal dunes and beach sites in the study area are: Istirinchá (I), Lechuguillas (Le), El Morro (EM), Palma Sola (PS), Boca Andrea (BA), Villa Rica (VR), Farallón (F), La Mancha (LM), and Chachalacas (CH). The topography is more prominent in the central part than in the northern and southern coastal areas near the TMVB (Figs. 1 and 2). The coastal dune systems are characterized by transverse mobile and vegetated systems with average heights of 2–8 m in the northern area, and transverse-vegetated and dominant parabolic-barchanoid dunes in the southern area with average heights of ~ 10 m (Figs. 3A–C). A transgressive, low relief, narrow coastal plain (on average 1.25 km) with accretionary and wave-dominated beaches is observed along the coast of the WGM (Ortiz-Pérez and Espinosa, 1991).

The fluvial network includes ten perennial rivers located between Istirinchá (I) in the north and Chachalacas (CH) in the south (Fig. 2). The rest of the rivers are of intermittent character as shown in the Digital Elevation Model Map (DEM) (Servicio Geológico Mexicano, 2017) (Fig. 2). Some previous petrographic data are available for rivers close to the PS and CH sites (Kasper-Zubillaga et al., 1999).

The physical oceanography of the longshore currents shows a northward component in spring-summer with average velocities of 5.75 cm s^{-1} (3.5 to 8.0 cm s^{-1}) (Fernández-Eguiarte et al., 1992). Multi-directional winds are present as follows: a) northeasterly and easterly winds with average velocities of 4-6 m s^{-1} in summer, and b) northerly winds with average velocities of 8 m s^{-1} in the fall (Perez-Villegas, 1990). Waves average 0.90 m in height with 3–8 s periods. Tides are of diurnal and mixed-diurnal types with an average tidal range of 0.30 m.

2.1. Geology

The TMVB is the largest Neogene volcanic arc in North America, encompassing 160,000 km^2, with a length of almost 1000 km in central Mexico. It is a continental arc that exhibits significant variation in composition and volcanic style, with intra-arc extensional tectonics in the eastern part of continental Mexico close to the WGM coastal area. Here, the TMVB is characterized by mafic volcanism (Ferrari et al., 2011) (Figs. 1,2). Rocks are late Miocene (ca. 7.5 Ma) to early Pliocene (ca. 3 Ma) volcanic fields of Na-alkaline character with small volumes compared to volcanic contemporaneous calc alkaline (subalkaline) rocks close to the WGM coast (Cantagrel and Robin, 1979; Negendank et al., 1985; Gómez-Tuena et al., 2007). The coastal area is exposed by the volcanic fields near the Nautla and Chachalacas beach sites comprising andesites, andesites-dacites, basalts, volcanic tuffs, and basaltic breccias (Servicio Geológico Mexicano, 2017). In the northern area of the WGM, outcrops of rhyolite tuffs and pumice are exposed. Quaternary volcanic rocks are mainly calc-alkaline (subalkaline), although associated Na-alkaline lavas of basanitic to mugearitic intermediate composition (Fig. 2), e.g. clinopyroxene, Fe-rich olivine, oligoclase and opaque Ti-Fe-bearing minerals have also been reported (Muir and Tilley, 1961; Trumbull et al., 2003; Nonnotte et al., 2011). Quaternary sedimentary units are represented by alluvial and aeolian sands exposed along the coastal area.

3. Sampling, equipment, and analytical procedure

3.1. Sampling

Nine beach sites with CDs were sampled along the WGM coast. From north to south, the sites are known as Istirinchá (I), Lechuguillas (LE), El Morro (EM), Palma Sola (PS), Boca Andrea (BA), Villa Rica (VR), Farallón (F), La Mancha (LM), and Chachalacas (CH). Samples were taken from the stoss face (s; n = 14), the crest (c; n = 16), and the lee face (l = 9) of the coastal dunes, from the inshore (i = 3) and foreshore (f = 7) of the beach (total n = 49; Table 1). Our sampling avoided a bias effect by collecting sands in which heavy mineral lag deposits were observed, i.e. mainly opaque fractions. Only the upper part of the CD and beach sands were collected with a trowel (~ 140 g) to ensure that the sample corresponded to recent sediments, to avoid mixing with deep sand laminae deposits. Beach sands were sampled to determine the physical and chemical mechanisms that characterize the CD sands; this is documented in several papers where wind deflation, wave regime, and heavy mineral concentration from the beach influence the composition of CD sand (Kasper-Zubillaga et al., 2007; Garzanti et al., 2015).

3.2. Grain size parameters

Approximately 10 g of CD and beach sands was used for grain size determination. A Ro-Tap sieve shaker and American Standard Test Sieve Series (ASTM) were used with 0.5 ϕ intervals for size separation. Gradistat software was used to perform the grain-size calculations in the Microsoft Excel version 8.0 2000–2003 (Blott and Pye, 2001) http://www.kpal.co.uk/gradistat.html). Grain-size statistical parameter intervals were used to assess grain size patterns in the CD sands and some beach sands (Folk, 1980) (Table 1).

3.3. Wind speed measurements

A total of 126 wind speed measurements in m s^{-1} performed during field sampling by a Steren HER-440 handheld anemometer were carried out for each beach site: Istirinchá n = 37, Lechuguillas n = 11, El Morro n = 10, Palma Sola n = 10, Boca Andrea n = 10, Villa Rica = 12, El Farallón n = 11, La Mancha n = 11, and Chachalacas n = 14. Wind measurements began in the foreshore of the beach and continued progressively in the dune and back to the foreshore during beach and CD sand sampling.

3.4. Modal analysis

A Velab VE-148 P polarized microscope with 10 x objective was used for modal analysis. Five hundred points were counted in thin sections previously prepared with epoxy resin without cover slips for the CD and beach sands, using GazziDickinson's point counting method (Marsaglia, 1993; Garzanti et al., 2013a, 2013b). The first category (n = 250 grains per slide) included total quartz i.e. Q = all quartz grains, including single-crystal and polycrystalline quartz, total feldspar

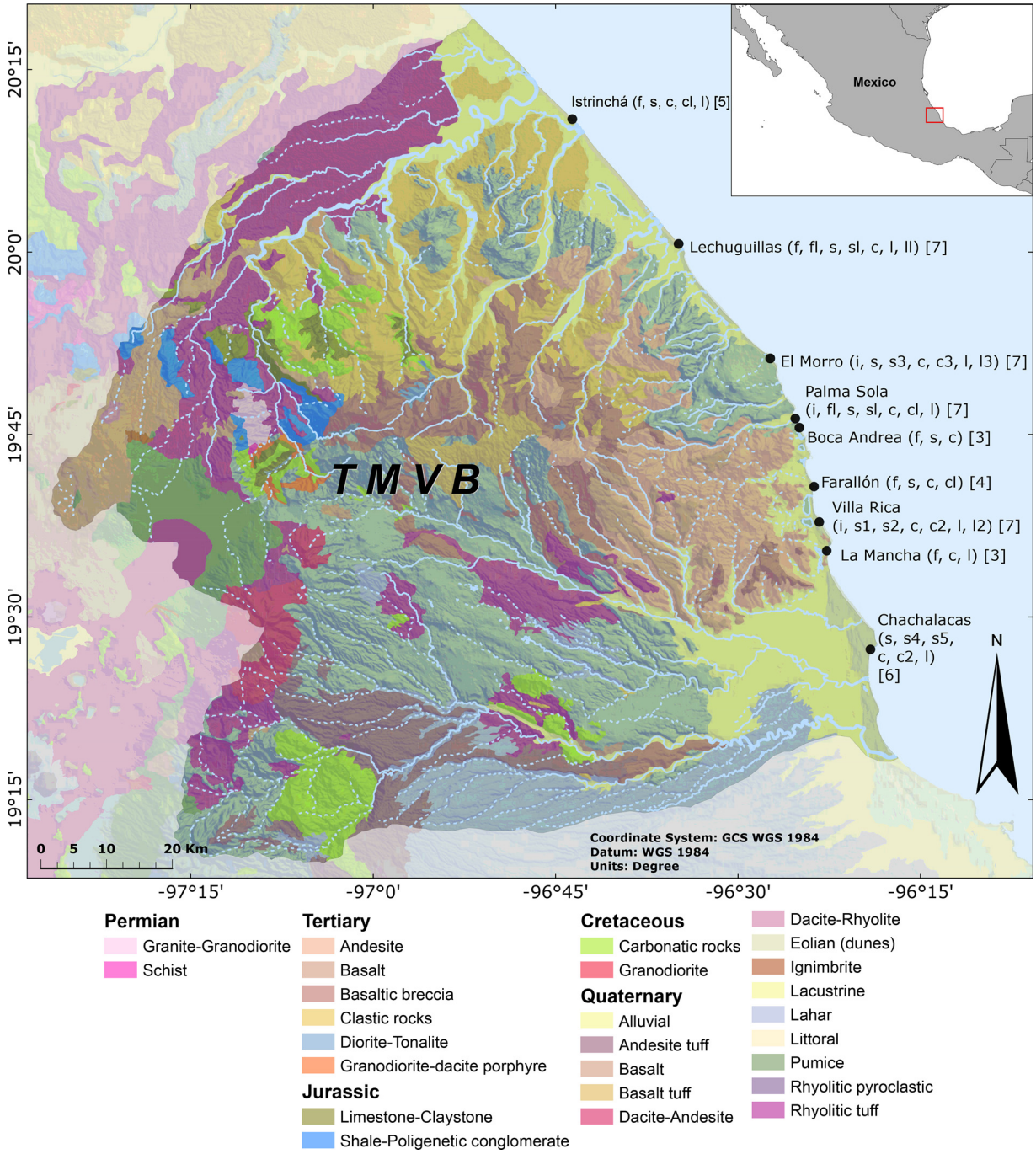

Fig. 1. Study area, sampling sites, and geology (modified from the Servicio Geológico Mexicano, 2017).

F = potash feldspar, plagioclase (P), and total lithics (L, volcanic and sedimentary; absence of metamorphic outcrops is observed). The second category (n = 250 grains per slide) included volcanic lithics with lathwork (Lvl), microlithic (Lvm), and vitric textures (Lvv), sedimentary lithics (Ls, including sandstones, siltstones, chert), heavy minerals (HM, including clinopyroxene (px), olivine (ol), amphibole (a), opaque minerals (op = mainly ilmenite), and biogenic components (B = calcite-composed shell fragments and foraminifera) (Marsaglia et al., 2016). Point counts were recalculated to percentages for each category. Ternary diagrams were constructed with the following poles a) Q-F-L; b) Lvl-Lvm-Lvv; c) ol-px-op. These diagrams were prepared to show: (a) general mineralogical composition, relief, parent rock, and the influence of coastal dynamics; (b) provenance of CD sands linked mainly to rapidly cooling lavas (Lvl, Lvv), andesitic-Na-alkaline lavas (Lvm), and probably rhyolitic tuff; (c) labile heavy-mineral loss associated with sub-humid warm weather and the influence of coastal dynamics (Table 2; Fig. 4A–C).

3.5. Geochemical analysis

We analyzed 30 sand samples for major and trace elements based on the aim of our work which considers mostly CD but also some beach sands to discuss the importance of the coastal dynamic processes controlling the sand composition. Sand samples were crushed in a Fritsch Pulverisette Grinding Mill Model 2, micro-milling from medium-hard to soft-brittle samples to obtain fine powders (particle size < 75 μm) to

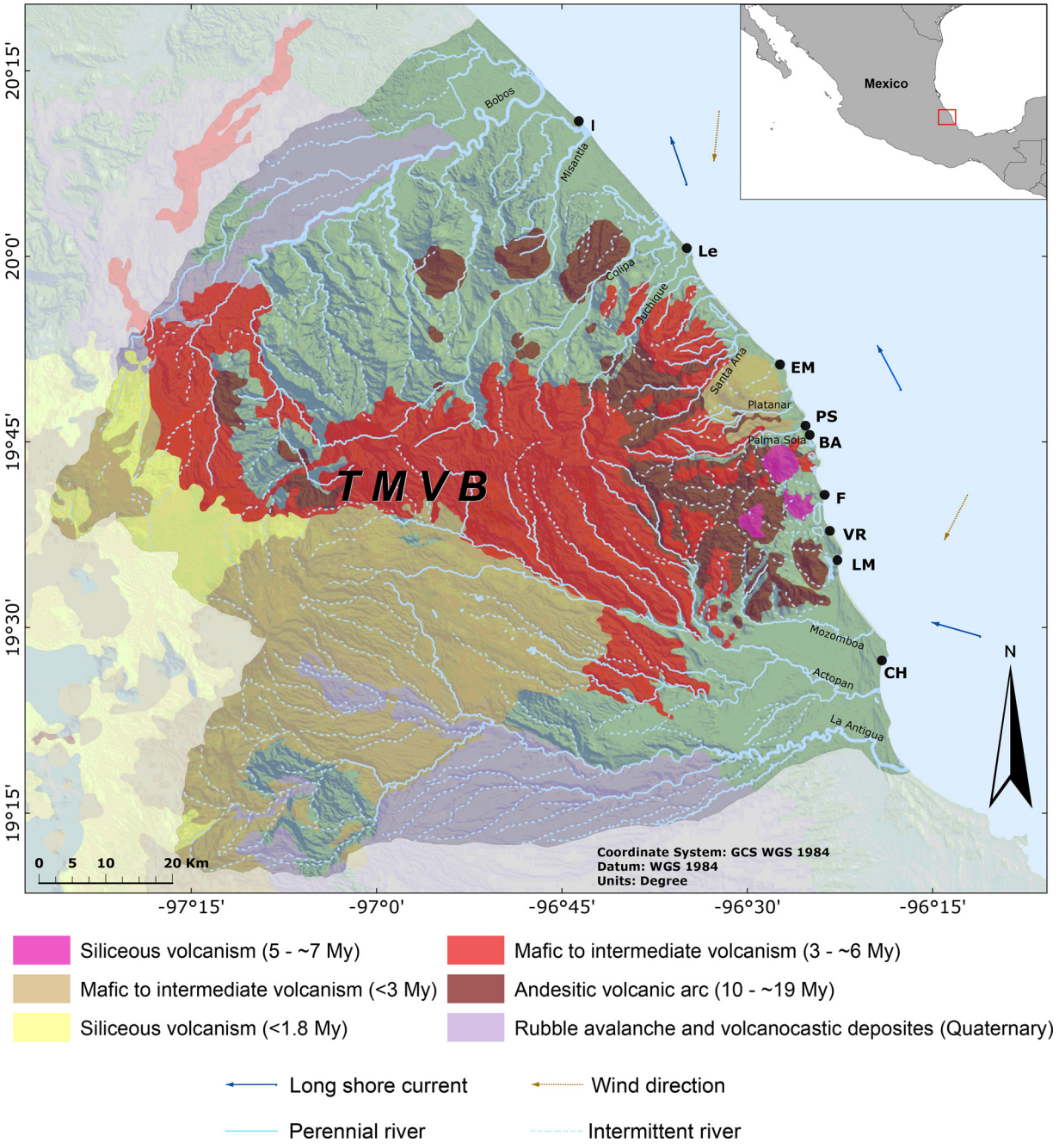

Fig. 2. Geomorphological map showing inferred intermittent and perennial rivers, dominant littoral currents, and wind direction in dark and dotted arrows. Beach sampling locations are shown in Table 1 for beach names, coordinates, and wind speeds. (modified from the Servicio Geológico Mexicano, 2017).

further analyze major and trace elements.

X-ray fluorescence analyses were performed with the powdered samples. After drying the samples at 110 °C for 6 h, they were heated in a muffle furnace at 1000 °C for 2 h to obtain a stable mass by LOI (loss on ignition). Fused beads were prepared from each calcined sample using a lithium tetraborate flux. Final analyses were carried out using a Rigaku model RIX-3000 equipped with Rh tube at the Instituto de Geología, Universidad Nacional Autónoma de México (UNAM). Calibration curves were determined using international reference materials, i.e. IGLA-1 andesite close to the composition of the CD and beach sands (Lozano and Bernal, 2005). The resulting chemical analyses for major elements show precisions better than 5%. Major element data were recalculated on an anhydrous (LOI-free) basis and adjusted to 100%. Highly variable values of LOI values are shown in Table 3. Major and trace elements were normalized against the Upper Continental Crust (UCC) (Taylor and Mc Lennan, 1985) (Tables 3 and 4). Absolute error (%) of major and trace elements for certified values are shown in Table 5.

3.6. Rare earth elements

Approximately 0.2 grams of sand samples were crushed to add HF and $HClO_4$. Samples were stored to permit evaporation and total sand dryness, and then we added 100 mL of HCO_3 (2%). The REE analysis was performed in an inductively-coupled plasma mass spectrometer (ICP-MS) model iCAP Qc Thermo Scientific at the Instituto de Geofísica, UNAM. Samples were digested with 2.5 ml HF ml in 0.5 g of crushed samples. They were stored with 4 ml of $HClO_4$ until desiccation was completed, followed by dilution with 50 ml of HNO_3 (2%). We weighed 0.2 g of samples and a mixed them with HF and $HClO_4$. Samples were

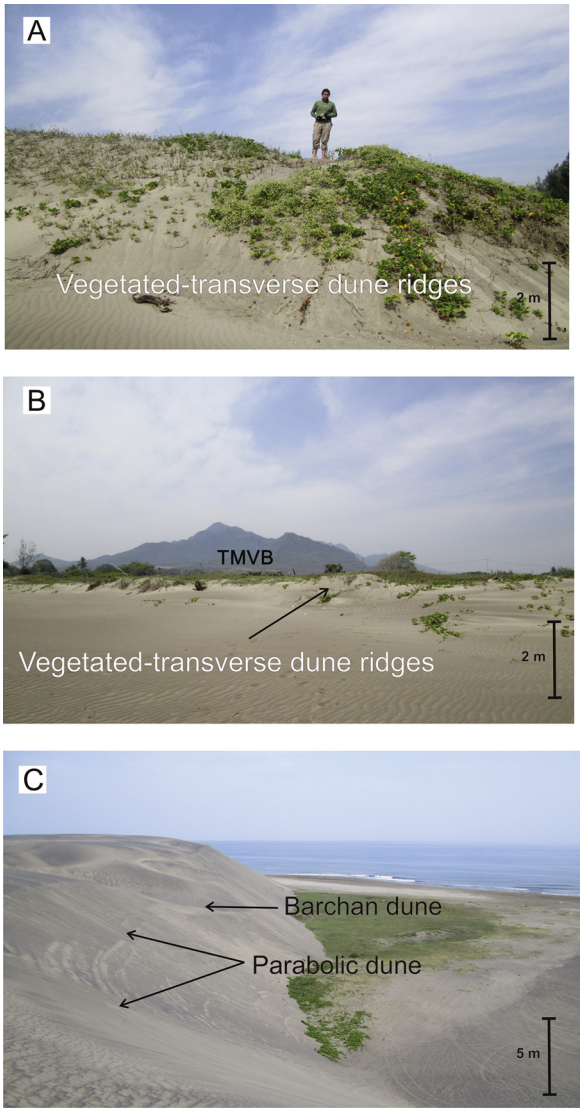

Fig. 3. (A, B). Vegetated transverse dune ridges at the Palma Sola (PS) and Boca Andrea (BA) sites (PS); (C) barchan and parabolic dunes at the Chachalacas site "(CH) height is m.

dried and we added 100 ml of HNO_3 (2%). The ICP-MS instrument was optimized with a certified High-Purity Standard (SM-1595-143) solution with a broad range of Li, Co, In, Ba, Bi, Ce, and U of 1 µg/L. The calibration curve was plotted for 14 points (0, 0.1, 0.25, 0.5, 0.75, 1, 2.5, 5, 7.5, 10, 25, 50, 75, and 100 µg/L) starting with a multi-elemental stock of 10 mg/l of an additional High-Purity Standard (ICP-MS-B). Instrumental drift correction was performed using 10 µg/L of an internal standard. Detection limits (DLs) were calculated with the following formula: DL = 3 (SD int BCO)(conc STD)/(int STD - aver int BCO); where SD int BCO is the standard deviation of the blank intensity, conc STD is the standard solution concentration, int STD is the standard solution intensity, and aver int BCO is the mean blank intensity. A basalt reference BCU-3 was used as a reference quality material for the ICP-MS analysis.

3.7. Normalization of REE and Ce/Ce*, Eu/Eu* anomalies

Normalization against the UCC of REE data in ppm was performed following the values indicated in Taylor and Mc Lennan (1985) (Fig. 7). Cerium and europium anomalies were calculated with $Ce/Ce^* = 3(Ce_N/2(La_N + Nd_N)$ and $Eu/Eu^* = Eu_n/[(Sm_n)(Gd_n)]1/2$; where subscript N is the normalized value for each element inserted into the equations (Table 5).

3.8. Weathering rates of CD and beach sands

To evaluate these chemical weathering rates and plagioclase depletion in CD and beach sands from the WGM coast, four estimations were applied: (1) The Chemical Index of Alteration (CIA), $CIA = 100 \times Al_2O_3/(Al_2O_3 + CaO^* + Na_2O + K_2O)$, which evaluates weathering intensity in rocks and old and modern sands and has proven to be a reliable indicator of chemical weathering in CD and beach sands (Nesbitt and Young, 1982; Kasper-Zubillaga et al., 2007; Carranza-Edwards et al., 2009; Carranza-Edwards et al., 2018); (2) The Plagioclase Index of Alteration (PIA), $PIA = [Al_2O_3 - K_2O/(Al_2O_3 + CaO^* + Na_2O)] \times 100$, where CaO* is part of the silicate fraction determined by the plagioclase depletion of the sands that is associated with climatic conditions in a sedimentary basin (Fedo et al., 1995; Fiantis et al., 2010). The CaO* was calculated using the equation CaO* 0.35 *2 mol (wt% of Na_2O/ Na_2O atomic molecular weight = 62) (McLennan, 1993); (3) The Chemical Index of Weathering (CIW), $CIW = 100x [(Al_2O_3/Al_2O_3 + CaO + Na_2O)]$, which measures the degree of feldspars converting into clay minerals (Fiantis et al., 2010); (4) The Weathering Index of Parker (WIP), $WIP = 100 (2Na_2O/0.35 + (Mg/0.9) + 2K_2O/0.25) + (Ca/0.7)$, which is a suitable index for studying the mobility of alkaline and alkaline earth metals, although it overestimates the degree of weathering in polycyclic quartzose sands due to the quartz dilution effect (Parker, 1970; Price and Velbel, 2003) (Table 6).

3.9. X-ray powder diffraction analysis

The mineralogy of four samples (I (s), PS (l), LM (l), and CH (c)) was determined by an Empyrean diffractometer (XRD). Samples were ground with an agate pestle and mortar to a fine powder in preparation for powder X-ray diffraction analysis. Diffractograms were recorded in step-scan mode of 0.003°, from a start angle of (2θ) 5.0° to an end angle of (2θ) 70.0°, with a time per step of 40 s. Diffraction data were stored after the initial X-ray exposure. Samples showed no significant evidence of degradation within the X-ray beam (Table 7).

4. Results

4.1. Grain size and sorting

Textural parameters showed that the CD and beach sands are medium-to-fine moderately-well-sorted sands with average values of Mz = 2.20 ϕ ± 0.27, sorting σ = 0.50 ± 0.10, and Mz = 2.10 ϕ ± 0.25, sorting σ = 0.56 ± 0.11 respectively. The average sand sizes are medium in Villa Rica with 1.89 ϕ ± 0.16, while average sand sizes in El Morro and Palma Sola are 2.45 ± 0.24, 0.25. Average sorting values (σ; ϕ) are 0.43 ± 0.07 in El Morro and Palma Sola but 0.62 ± 0.05 in Chachalacas. Northern sands from Istirinchiá to Boca Andrea are fine sizes between 2.26 ϕ ± 0.11 to 2.34 ϕ ± 0.19. In contrast, a slight sand size coarsening was observed in Villa Rica, i.e. 1.89 ± 0.55, and in Chachalacas 2.20 ± 0.13. Well-sorted, moderately-well-sorted to moderately-sorted CD and beach sands defined the overall granulometric characteristics.

4.2. Modal analysis

The CD sand samples extend their fields towards the Q and L poles while the beach sand group is in the middle sector of the diagram, e.g. beach sands I (f), Le (f), Le (f1), PS (i), PS (f1), BA (f), VR (i), and F (f) with the exceptions of beach sands EM (i) and LM (f). Angular to subrounded single-crystal altered quartz with some overgrowths was preserved over polycrystalline quartz (Figs. 4A, Figure 5A– F). A grouping

Table 1
Sampling sites, grain size and sorting of CD and beach sands (n = 49).

Sample	Environment	Longitude	Latitude	Average *in situ* wind speed (ms^{-1})	Mz (ϕ)	Sorting (ϕ)	Mz (ϕ)	Sorting (ϕ)
l (f)	Beach	96° 43' 38.8320" W	20° 10' 56.6580" N	2.87 ± 2.46	2.36	0.55	Fine sand	Moderately well sorted
I (s)	Dune				2.16	0.57	Fine sand	Moderately well sorted
I (c)	Dune				2.39	0.51	Fine sand	Moderately well sorted
l (c1)	Dune				2.25	0.54	Fine sand	Moderately well sorted
I (l)	Dune				2.15	0.58	Fine sand	Moderately well sorted
Le (f)	Beach	96° 42' 37.7972" W	20° 09' 50.6080" N	8.61 ± 1.03	1.68	0.45	Medium sand	Well sorted
Le (f1)	Beach				2.31	0.62	Fine sand	Moderately well sorted
Le (s)	Dune				2.24	0.53	Fine sand	Moderately well sorted
Le (s1)	Dune				2.13	0.59	Fine sand	Moderately well sorted
Le (c)	Dune				2.29	0.49	Fine sand	Well sorted
Le c(1)	Dune				2.39	0.46	Fine sand	Well sorted
Le (l1)	Dune				2.37	0.45	Fine sand	Well sorted
EM (i)	Beach	96° 27' 23.0100" W	19° 51' 20.5040" N	1.57 ± 0.25	2.00	0.51	Medium sand	Moderately well sorted
EM (s)	Dune				2.50	0.43	Fine sand	Well sorted
EM (s3)	Dune				2.25	0.50	Fine sand	Moderately well sorted
EM (c)	Dune				2.53	0.47	Fine sand	Well sorted
EM (c3)	Dune				2.72	0.32	Fine sand	Very well sorted
EM (l)	Dune				2.46	0.45	Fine sand	Well sorted
EM(l3)	Dune				2.73	0.34	Fine sand	Very well sorted
PS (i)	Beach	96° 25' 16.9500" W	19° 46' 18.6830" N	6.64 ± 0.94	2.23	0.50	Fine sand	Well sorted
PS (f1)	Beach				2.28	0.47	Fine sand	Well Sorted
PS (s)	Dune				1.89	0.51	Medium sand	Moderately well sorted
PS(s1)	Dune				2.50	0.33	Fine sand	Very well sorted
PS (c)	Dune				2.00	0.56	Fine sand	Moderately well sorted
PS(c1)	Dune				2.40	0.29	Fine sand	Very well sorted
PS (l)	Dune				2.45	0.43	Fine sand	Well sorted
BA (f)	Beach	96° 25' 16.9500" W	19° 46' 18.6830" N	5.17 ± 1.18	2.08	0.54	Fine sand	Moderately well sorted
BA (s)	Dune				2.55	0.33	Fine sand	Very well sorted
BA (c)	Dune				2.38	0.45	Fine sand	Well sorted
VR (i)	Beach	96° 23' 44.8500" W	19° 40' 44.0220" N	2.40 ± 1.00	2.23	0.55	Fine sand	Moderately well sorted
VR(s1)	Dune				1.88	0.53	Medium sand	Moderately well sorted
VR (s2)	Dune				1.78	0.54	Medium sand	Moderately well sorted
VR (c)	Dune				1.80	0.65	Medium sand	Moderately well sorted
VR(c2)	Dune				1.92	0.53	Medium sand	Moderately well sorted
VR (l)	Dune				1.92	0.54	Medium sand	Moderately well sorted
VR (l2)	Dune				1.74	0.50	Medium sand	Well sorted
F (f)	Beach	96° 23' 19.5000" W	19° 37' 49.7410" N	2.08 ± 0.84	2.17	0.53	Fine sand	Moderately well sorted
F (s)	Dune				2.17	0.53	Fine sand	Moderately well sorted
F (c)	Dune				1.74	0.47	Medium sand	Well sorted
F (c1)	Dune				2.24	0.51	Fine sand	Moderately well sorted
LM (f)	Beach	96° 22' 42.5300" W	19° 35' 27.1500" N	2.13 ± 0.47	1.65	0.84	Medium sand	Moderately sorted
LM (c)	Dune				2.20	0.57	Fine sand	Moderately well sorted
LM (l)	Dune				2.50	0.43	Fine sand	Well sorted
CH (s)	Dune	96° 19' 06.6600" W	19° 27' 20.8030" N	3.13 ± 1.02	2.06	0.55	Fine sand	Moderately well sorted
CH (s4)	Dune				1.94	0.62	Medium sand	Moderately well sorted
CH (s5)	Dune				2.19	0.58	Fine sand	Moderately well sorted
CH (c)	Dune				2.09	0.61	Fine sand	Moderately well sorted
CH (c2)	Dune				1.82	0.69	Medium sand	Moderately sorted
CH (l)	Dune				2.01	0.68	Fine sand	Moderately well sorted

See text for names of each location shown by capital letters. Longitude and latitude is shown for the first site sampled. Subenvironment sites are beach: i = inshore, f = foreshore, dune: s = stoss, c = crest, l = lee face. Numbers after subenvironment sites represent progressive sampling along the coast. Wind speed in ms^{-1} are average *in situ* measurements; see subsection Wind speed measurements for further explanation.

of CD and beach sand samples is presented in Fig. 4A. Some northern samples tend towards the Q pole, such as samples from Istirinchiá, Lechuguillas, El Morro, and Boca Andrea.

Plagioclase was scarce and only preserved as a single crystal within volcanic lithics with lathwork texture (Fig. 5C). The volcanic lithic compositions are $Lvl_{78}Lvm_{10}Lvv_{12}$ and $Lvl_{85}Lvm_{7}Lvv_{8}$ for the CD and beach sands respectively. The Lvl-Lvm-Lvv shows that the CD sand samples are irregularly distributed towards the Lvl and Lvm poles whereas the beach sands are concentrated towards the Lvl pole with the exception of sample Le (f). Volcanic lithics with lathwork textures were dominant in the whole bulk composition of the CD and beach sands i.e. Lvl < Lvm < lvv (Figs. 4 B, Figure 5B, C). Volcanic lithics dominate the CD and beach sand composition compared to Ls as we report the average Lvl + Lvm + Lvv = 84 ± 36 and Ls = 61 ± 29 (Table 2). The Lvl-Lvm-Lvv showed little grouping of CD and beach sand samples with some dispersed samples from the northern sites such as Istirinchiá, Lechugillas, and Chachalacas, close to the Lvl fractions pole. Our interpretation suggests that the high concentration of the samples towards the Lvl poles corresponds to high energy environments with dynamic longshore currents.

The heavy mineral associations are $ol_{2}px_{58}op_{40}$ for the CD, and $ol_{2}px_{61}op_{37}$ for the beach sands. The ol-px-op ternary diagram shows a trend for the northern CD and beach sand samples towards the op-pole while subordinate olivine was scarce as a single crystal in the whole bulk CD and beach sands (Figs. 4C, Figure 5B, D). Sub-rounded ilmenite was abundant in the northern locations (I, Le, and EM) (Figs. 4C, Figure 5A). The HM associations group opaque minerals in the Istirinchiá, Lechugillas and El Morro sites, while the rest of the minerals, i.e. px and ol, tend towards the rest of the localities (Fig. 4C). Biogenic fractions were abundant in the whole bulk composition and some foraminifera were present in the beach sands, i.e. sample PSm2 (Fig. 5B).

Table 2
Modal analysis of CD and beach sands from the WGM (= 49).

Sample	Qm	Qp	Fk	P	Lt	HM	B	Total	Lvl	Lvm	Lvv	Ls	ol	px	a	op	Total
l (f)	53	1	0	1	35	84	76	250	53	4	8	19	0	69	2	95	250
I (s)	72	0	0	0	20	54	104	250	35	2	18	34	1	80	4	76	250
I (c)	89	4	0	2	35	77	43	250	39	5	18	29	1	67	1	90	250
l (c1)	83	0	0	0	28	37	102	250	63	1	9	23	6	35	0	113	250
I (l)	76	6	0	3	30	88	47	250	13	4	9	52	1	70	5	96	250
Le (f)	58	3	0	2	49	24	114	250	44	9	19	65	0	80	7	26	250
Le (f1)	26	0	0	0	15	181	28	250	22	2	1	6	0	68	0	151	250
Le (s)	100	2	1	0	29	57	61	250	25	4	7	38	2	107	4	63	250
Le (s1)	78	0	0	0	39	72	61	250	31	3	3	14	1	54	0	144	250
Le (c)	113	0	1	2	36	46	52	250	36	4	10	37	1	83	8	71	250
Le c(1)	42	0	0	0	37	88	83	250	48	2	1	15	0	33	0	151	250
Le (l1)	82	1	0	2	25	79	61	250	27	4	13	40	0	78	3	85	250
EM (i)	58	2	0	2	95	6	87	250	87	7	4	117	2	16	0	17	250
EM (s)	113	0	0	0	35	57	45	250	29	3	9	34	2	75	2	96	250
EM (s3)	77	2	0	0	29	19	123	250	73	0	0	25	0	51	0	101	250
EM (c)	112	0	1	0	21	72	44	250	19	0	6	25	0	96	9	95	250
EM (c3)	110	0	0	2	24	72	42	250	93	1	3	31	1	73	0	48	250
EM (l)	117	0	1	0	30	69	33	250	47	1	12	27	1	60	2	100	250
EM (l3)	122	1	0	1	18	75	33	250	38	2	4	44	3	72	1	86	250
PS (i)	94	2	0	5	56	56	37	250	83	2	13	17	0	94	8	33	250
PS (f1)	96	0	0	1	50	11	92	250	161	19	2	58	0	6	0	4	250
PS (s)	99	2	1	1	69	24	54	250	83	12	11	25	0	86	9	24	250
PS(s1)	103	0	0	0	46	11	90	250	135	0	1	18	0	53	3	40	250
PS (c)	50	1	0	0	90	15	94	250	95	6	13	36	0	56	12	32	250
PS(c1)	101	0	0	0	43	8	98	250	131	6	5	36	0	30	0	42	250
PS (l)	120	2	0	3	57	17	51	250	82	8	46	24	2	57	1	30	250
BA (f)	98	0	0	0	42	43	67	250	92	12	3	36	0	59	1	47	250
BA (s)	123	6	0	2	35	54	30	250	46	8	21	41	1	79	3	51	250
BA (c)	101	3	1	2	54	56	33	250	111	4	8	5	1	71	5	45	250
VR (i)	89	0	0	0	79	10	72	250	141	9	13	26	1	31	4	25	250
VR(s1)	26	5	0	2	29	33	155	250	82	1	10	49	2	56	0	50	250
VR (s2)	46	5	0	6	76	42	75	250	80	9	4	17	2	91	19	28	250
VR (c)	41	0	0	0	52	83	74	250	46	0	3	18	4	130	0	49	250
VR (c2)	56	3	0	2	55	29	105	250	84	15	2	34	1	61	0	53	250
VR (l)	37	3	0	2	74	43	91	250	103	5	5	29	0	82	11	15	250
VR (l2)	85	3	0	2	57	17	86	250	94	9	8	36	3	64	6	30	250
F (f)	74	2	1	3	41	62	67	250	73	1	6	45	6	101	1	17	250
F (s)	70	1	0	1	57	56	65	250	90	7	3	24	0	94	11	21	250
F (c)	77	0	0	2	56	74	41	250	50	5	5	21	2	121	6	40	250
F (c1)	83	0	1	1	42	38	85	250	38	6	4	75	14	87	1	25	250
LM (f)	47	0	0	0	96	36	71	250	99	6	3	27	5	96	7	7	250
LM (c)	68	0	0	0	65	36	81	250	76	13	4	38	0	79	10	30	250
LM (l)	129	1	0	0	24	26	70	250	100	15	4	37	1	75	4	14	250
CH (s)	73	0	0	0	77	19	81	250	45	25	3	70	4	86	0	17	250
CH (s4)	41	17	0	2	89	15	86	250	54	42	9	98	3	39	0	5	250
CH (s5)	98	0	0	1	49	28	74	250	48	16	14	128	5	24	0	15	250
CH (c)	88	0	0	0	61	24	77	250	38	42	7	130	3	24	0	6	250
CH(c2)	101	0	0	0	71	7	71	250	87	2	9	100	0	34	10	8	250
CH (l)	38	11	0	0	79	56	66	250	80	25	8	51	2	51	0	33	250
Average	80.27	1.82	0.16	1.12	49	46.65	70.98	250	68.35	7.92	8.18	41.31	1.71	67.02	3.67	51.84	250
Standard deviation	27.71	3.11	0.37	1.36	21.66	31.69	26.45	0	34.31	9.29	7.5	29.28	2.44	26.63	4.34	39.47	0

Qm = monocrystalline quartz; Qp = polycrystalline quartz; Fk = K-feldspar; P = Ca-Na plagioclase; Lt = total lithics (volcanic and sedimentary, absence of metamorphic lithics is observed); HM = heavy minerals (opaque and translucid); B = biogenic fractions (rest of mollusks, foraminifera); Lvl = lathwork volcanic fragments; Lvm = microlithic volcanic fragments; Lvv = vitric volcanic fragments; Ls = sedimentary lithics (sandstones, siltstone, chert); ol = olivine (fayalite); px = clinopyroxene; a = amphibole; op = opaque (ilmenite). Point counts are 250 grains per sample in two categories (Gazzi-Dickinson Method, see text for details). See Table 1 for abbreviations and sampling codes.

4.3. Major and trace elements of CD and beach sands

The major element data showed that CD and beach sands are superimposed with high content near/above the UCC line of SiO_2, TiO_2, Al_2O_3, Fe_2O_3, MnO, and MgO. Depletion of CaO and an increase below the UCC line for Na_2O and K_2O was observed. Trace elements increased their concentrations above the UCC for V, Cr, Co, and Ni in both CD and beach sands (Fig. 6A, B). Homogeneous major element trends were observed in all localities. Trace elements show a conspicuous trend towards V, Cr, Co values above the UCC line, especially at the Istiriinchiá and Villa Rica sites.

4.4. Spearman rank correlation (SRC; r_s) of mineralogy and major element data

A SRC was performed for CD and beach sand samples. Significant positive and negative correlations for an r_s with $\rho < 0.05$ and n-2 = 28 showed r_s values < 0.37. Significant correlations based on direct relationships between modal mineralogy and geochemistry of major and trace elements were as follows: Qm vs. SiO_2, $r_s = 0.60$; HM vs. TiO_2, $r_s = 0.61$; HM vs. Fe_2O_3, $r_s = 0.57$; B vs. CaO $r_s = 0.42$; op vs. HM, $r_s = 0.66$; py vs. Mg, $r_s = 0.47$; HM vs. V, $r_s = 0.62$; HM vs. Cr, $r_s = 0.47$; HM vs. Co, $r_s = 0.42$. A significant correlation of $r_s = 0.92$ was found between LOI and CaO.

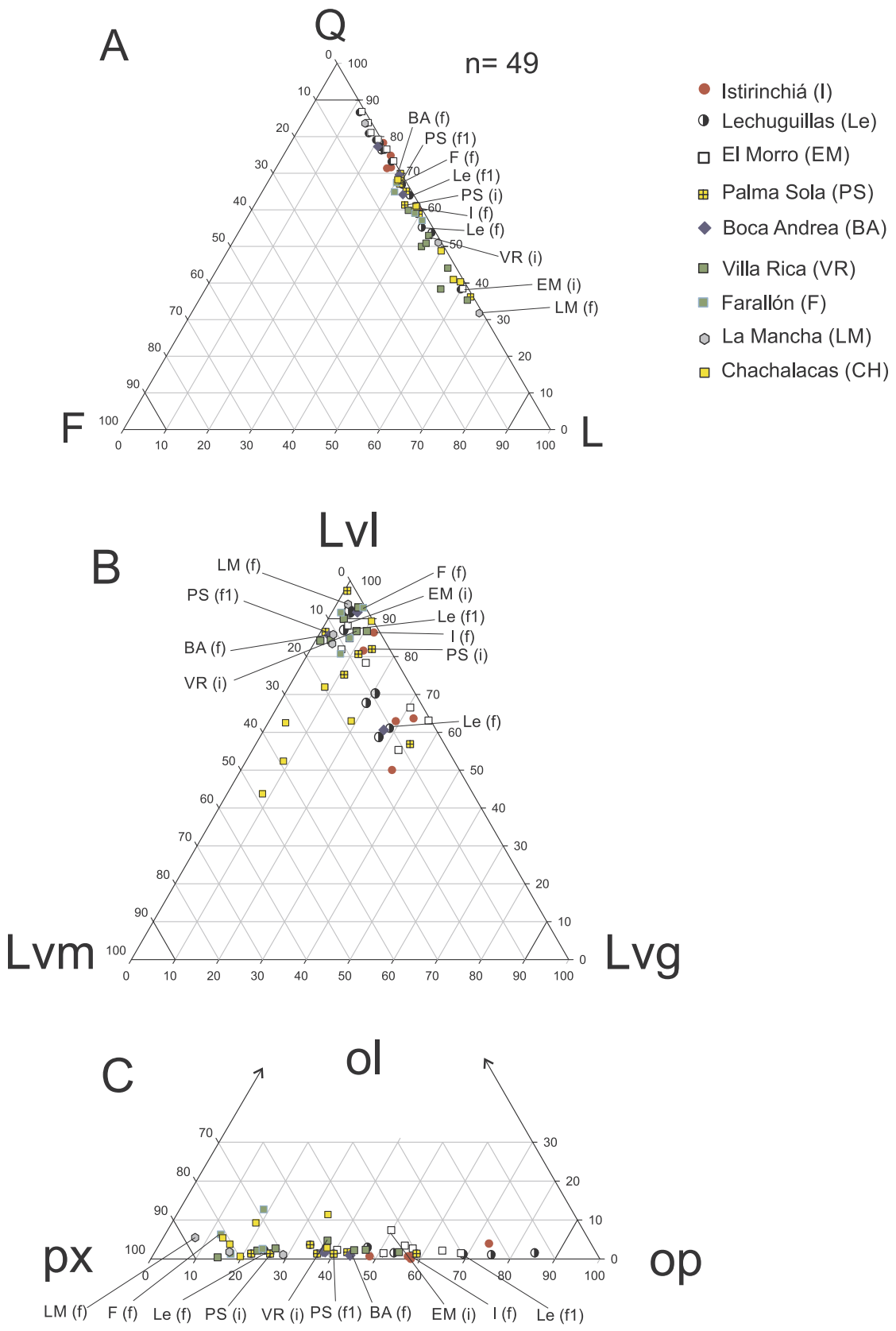

Fig. 4. Ternary plots showing **(A)** Q-F-L; **(B)** Lvl-Lvm-Lvv; and **(C)** ol-py-op modal analyses. See text for explanation of the samples shown in the diagrams.

Table 3
Major element concentration in weight % for the CD and beach sands (n = 30).

Sample	SiO_2	TiO_2	Al_2O_3	Fe_2O_3	MnO	MgO	CaO	Na_2O	K_2O	P_2O_5	LOI	Total (%)
I (s)	38.95	1.28	5.27	7.77	0.15	3.11	24.51	0.9	0.64	0.14	17.07	99.77
I (c)	46.41	2.33	5.64	12.63	0.18	3.46	16.86	1	0.73	0.14	10.52	99.89
I (l)	40	1.96	5.3	11.35	0.19	3.84	21.51	0.85	0.61	0.16	14.08	99.84
Le (f)	43.74	0.76	7.04	5.37	0.12	3.79	22.12	1.38	0.91	0.17	14.48	99.88
Le (s)	55.2	1.15	7.05	6.85	0.12	3.09	14.62	1.43	1.02	0.14	9.2	99.88
Le (c)	57.74	1.15	7.41	6.41	0.11	3.04	13.33	1.51	1.05	0.14	7.99	99.88
Le (l1)	57.12	1.25	7.12	6.79	0.12	3.23	13.6	1.44	1.01	0.14	8.06	99.88
EM (i)	50.37	0.43	7.04	2.87	0.07	1.58	19.94	1.53	1.09	0.12	14.85	99.88
EM (s)	55.88	1.01	6.28	5.38	0.1	2.79	15.76	1.21	0.97	0.12	10.38	99.77
EM (c)	56.76	1.09	6.2	6.14	0.1	2.7	14.77	1.24	1.02	0.12	9.65	99.88
EM (l)	58.51	0.71	6.69	4.33	0.08	2.3	14.73	1.4	1.1	0.12	9.91	99.8
PS (i)	50.61	0.53	6.27	3.44	0.08	1.93	19.94	1.33	0.99	0.11	14.64	99.87
PS (s)	41.53	0.5	6.75	3.71	0.09	2.23	24.42	1.36	1.02	0.14	18.03	99.78
PS (c)	46.45	0.51	6.94	3.54	0.08	2.12	21.71	1.4	1.06	0.13	15.94	99.88
PS (l)	62.71	0.41	7.51	2.6	0.06	1.54	12.82	1.6	1.31	0.1	9.23	99.87
BA (s)	73.44	0.44	6.72	2.69	0.05	1.88	7.5	1.49	1.28	0.08	4.31	99.88
BA (c)	74.69	0.51	7.4	2.2	0.04	1.4	6.57	1.66	1.32	0.09	4.02	99.88
VR (i)	58.83	0.46	7.45	2.42	0.06	1.31	14.95	1.62	1.35	0.11	11.34	99.88
VR (s)	52.35	0.65	7.55	4.67	0.09	3.52	17.55	1.52	1.05	0.14	10.98	99.78
VR (c)	40.09	1.22	6.09	8.51	0.14	5.78	23.16	1.02	0.67	0.14	13.07	99.88
VR (l)	54.15	0.67	7.55	4.25	0.09	3.13	16.73	1.54	1.08	0.14	10.56	99.87
F (f)	47.19	0.71	5.96	4.32	0.09	2.84	21.61	1.11	0.87	0.12	15.06	99.87
F (s)	40.67	0.63	5.91	5.12	0.11	4.93	25.1	1.03	0.69	0.12	15.59	99.88
F (c)	47.09	0.68	6.09	4.93	0.11	4.14	21.34	1.14	0.84	0.13	13.4	99.88
LM (f)	50.48	0.83	8.15	5.51	0.1	5.18	17.68	1.58	1.03	0.18	9.16	99.88
LM (c)	42.58	0.82	5.44	4.65	0.1	3.01	24.23	0.96	0.75	0.12	17.22	99.88
LM (l)	57.68	0.56	6.18	3.17	0.07	2.04	16.17	1.22	1.09	0.1	11.6	99.88
CH (s)	54.83	0.93	9.53	5.37	0.09	3.4	13.89	1.92	1.34	0.2	8.39	99.88
CH (c)	53.9	0.88	9.4	5.1	0.09	3.02	14.67	1.87	1.31	0.18	9.46	99.87
CH (l)	55.99	0.64	9.67	4.16	0.08	2.35	13.98	1.97	1.44	0.17	9.44	99.88
Average	52.20	0.86	6.92	5.21	0.10	2.96	17.53	1.37	1.02	0.13	11.59	99.86
Standard deviation	8.94	0.44	1.15	2.42	0.03	1.10	4.82	0.29	0.23	0.03	3.59	0.04

See Table 1 for abbreviations; LOI = Loss on Ignition.

Table 4
Trace elements in ppm for the CD and beach sands (n = 30).

Sample	Rb	Sr	Ba	Y	Zr	Nb	V	Cr	Co	Ni	Cu	Zn	Th	Pb
I (s)	20	436	200	25	118	12	104	106	29	26	6	71	7	10
I (c)	21	328	105	24	359	27	217	137	54	26	4	101	7	12
I (l)	18	379	106	26	269	19	176	149	42	29	4	94	7	11
Le (f)	25	481	299	25	88	8	78	107	22	40	10	54	6	9
Le (s)	28	372	343	21	169	11	117	125	24	30	8	59	6	9
Le (c)	26	494	318	25	109	11	73	185	24	33	8	48	7	9
Le (l1)	28	356	341	20	168	12	125	129	23	32	9	63	5	8
EM (i)	32	495	365	22	76	10	42	41	21	20	8	39	5	8
EM (s)	29	369	374	20	135	12	97	167	31	28	7	51	5	6
EM (c)	30	361	370	20	176	13	116	175	25	29	7	54	4	10
EM (l)	31	380	386	20	104	10	75	116	20	25	7	43	5	7
PS (i)	29	446	376	21	90	9	51	179	18	23	6	38	4	8
PS (s)	29	527	336	24	75	7	49	84	20	26	9	44	5	9
PS (c)	30	490	348	24	78	9	49	66	19	25	8	42	5	8
PS (l)	37	375	436	19	84	13	42	43	22	18	6	33	5	9
BA (s)	36	283	442	15	80	8	53	64	13	22	6	27	5	9
BA (c)	38	298	510	14	87	13	47	60	21	18	6	27	4	7
VR (i)	40	419	417	20	81	11	40	26	20	19	7	36	6	8
VR (s)	28	435	427	20	87	12	74	223	27	38	9	46	5	8
VR (c)	19	418	350	18	133	11	138	635	34	58	11	62	6	9
VR (l)	31	427	396	20	89	8	71	168	21	34	10	43	6	7
F (f)	26	438	337	22	85	9	64	152	20	30	6	42	5	9
F (s)	20	457	340	21	62	7	71	343	24	48	8	41	3	8
F (c)	25	423	334	22	73	9	74	216	24	40	8	45	4	9
LM (f)	26	442	439	18	93	11	93	362	26	52	13	47	6	9
LM (c)	27	341	354	20	144	10	106	115	20	29	7	54	5	7
LM (l)	33	380	355	20	88	9	53	72	19	24	7	35	5	9
CH (s)	36	467	471	21	126	14	95	174	24	41	13	50	6	8
CH (c)	36	473	441	22	120	12	86	144	20	37	12	50	6	8
CH (l)	39	476	446	22	114	10	71	87	18	32	12	45	8	9
Average	29.10	415.53	358.73	21.03	118.67	11.23	84.90	155.00	24.17	31.07	8.07	49.47	5.43	8.57
Standard deviation	6.05	61.55	91.26	2.76	62.23	3.84	40.57	119.39	7.85	9.80	2.38	16.47	1.10	1.22

Table 5
Recovery (%) for Mv average measured samples (this study) compared to certified standards (Cv).

Major elements	Recovery %	Trace elements	Recovery %
SiO2	100.39	Rb	98.50
TiO2	100.13	Sr	99.22
Al2O3	99.38	Ba	100.14
Fe2O3t	100.31	Y	97.58
MnO	102.09	Zr	98.45
MgO	103.24	Nb	95.52
CaO	100.24	V	92.41
Na2O	103.77	Cr	103.13
K2O	100.33	Co	110.89
P2O5	99.89	Ni	92.48
		Cu	102.45
		Zn	92.66
		Th	111.78
		Pb	101.66

Cv = IGLA-1 certified standards; R% recovery = Mv average measures samples [(Mv-Cv)*100].

4.5. REE for CD and beach sand samples

The REE analyses for the three sites are given in Table 5 and the UCC normalized patterns are presented in Fig. 6C. The REE/UCC horizontal patterns are similar to those observed in beach sands near volcanic rock input, i.e. Tacaná volcano in southeastern Mexico (Carranza-Edwards et al., 2018). There is a depletion of light REE concentration compared to heavy REEs. Negative and positive Ce ~ 0.61-0.67 and Eu ~ 1.14–1.40 anomalies were determined for the CD and beach sands (Fig. 6c). Most of the samples showed similar trends regardless of the sampling settings.

4.6. Weathering rates of the CD and beach sands: the CIA, PIA, CIW, and WIP indices

Results obtained from the CIA, PIA, CIW, and WIP indices are shown in Table 6. The CIA indicates the extent of conversion of feldspar to clays such as kaolinite expressed in molar concentrations. The CIA shows the leaching of alkalis in poles CN = Ca^{+2}; Na^{+}, K = K^{+} and A = Al^{+} and concentration of Al and Si in the residue (Goldberg and Humayun, 2010). The mean CIA value for the CD and beach sands of the WGM is 67.46 ± 2.13. The CIW measures weathering rates without considering the K_2O concentration as in the CIA. The PIA only monitors plagioclase depletions in the sands. In our study, both weathering measurements are useful as a result of the aim and assumed hypothesis in the expected weathering results of the CD and beach sands. The WIP

Table 7
Chemical Indices of CD and beach sands for the WGM.

Sample	A	CN	K	PIA	CIW	WIP
I (s)	70.81	19.89	9.30	64.53	67.69	23.79
I (c)	69.85	20.37	9.78	63.44	66.86	26.59
I (l)	72.03	19.00	8.97	66.14	69.05	24.99
Le (f)	68.38	22.06	9.56	61.09	64.60	33.15
Le (s)	67.09	22.40	10.51	59.80	63.82	32.69
Le (c)	67.17	22.53	10.30	59.78	63.71	33.68
Le (l1)	67.28	22.39	10.33	59.96	63.89	33.10
EM (i)	65.56	23.45	10.99	57.81	62.21	30.23
EM (s)	67.38	21.36	11.26	60.73	65.00	29.06
EM (c)	66.35	21.84	11.81	59.52	64.14	29.58
EM (l)	65.69	22.62	11.69	58.43	63.09	30.87
PS (i)	65.80	22.96	11.24	58.31	62.78	28.16
PS (s)	66.88	22.18	10.94	59.76	63.97	29.59
PS (c)	66.79	22.17	11.04	59.68	63.94	30.04
PS (l)	64.96	22.78	12.26	57.67	62.68	32.73
BA (s)	63.65	23.23	13.12	56.16	61.74	32.22
BA (c)	64.01	23.63	12.36	56.27	61.46	33.08
VR (i)	64.35	23.03	12.62	56.95	62.20	32.65
VR (s)	67.48	22.36	10.16	60.15	63.99	35.11
VR (c)	71.70	19.76	8.54	65.30	68.11	32.69
VR (l)	67.09	22.52	10.39	59.72	63.69	34.51
F (f)	68.28	20.93	10.79	61.80	65.76	27.26
F (s)	70.77	20.29	8.94	64.20	67.24	30.62
F (c)	68.62	21.14	10.24	61.92	65.65	30.91
LM (f)	68.69	21.92	9.39	61.44	64.86	40.17
LM (c)	69.47	20.17	10.36	63.30	66.97	25.08
LM (l)	65.98	21.43	12.59	59.45	64.44	28.12
CH (s)	67.40	22.35	10.25	60.09	63.97	41.58
CH (c)	67.65	22.15	10.20	60.43	64.27	39.74
CH (l)	66.82	22.41	10.77	59.57	63.72	40.08
Average	67.47	21.84	10.69	60.45	64.52	31.74
Standard deviation	47.68	26.24	26.08	2.53	1.91	4.49

See text for explanation of acronyms. A = aluminum; CN = calcium, sodium; K = potassium.

Table 6
REE elements in ppm for the CD and beach sands (n= 21).

Sample	La	Ce	Pr	Nd	Sm	Eu	Tb	Gd	Dy	Ho	Er	Tm	Yb	Lu	Ce/Ce*	Eu/Eu*
I (s)	19.26	35.97	4.92	20.57	4.13	1.02	0.53	3.82	3.30	0.64	1.78	0.24	1.58	0.23	0.63	1.21
I (c)	22.74	43.30	5.75	23.36	4.61	1.07	0.59	4.00	3.44	0.67	1.87	0.25	1.69	0.25	0.65	1.17
I (l)	26.30	53.14	6.99	28.28	5.44	1.23	0.65	4.69	3.91	0.74	2.06	0.28	1.86	0.28	0.67	1.14
Le (f)	15.32	29.65	4.18	18.08	3.92	1.03	0.60	3.69	3.08	0.59	1.64	0.22	1.40	0.20	0.63	1.27
Le (s)	14.78	28.79	3.90	15.90	3.37	0.92	0.49	3.07	2.56	0.49	1.38	0.19	1.18	0.17	0.65	1.34
Le (l1)	13.59	25.50	3.59	14.59	3.16	0.84	0.47	2.92	2.42	0.46	1.27	0.18	1.11	0.15	0.62	1.29
EM (i)	13.69	24.39	3.38	13.68	2.86	0.78	0.46	2.65	2.24	0.43	1.21	0.16	1.04	0.15	0.61	1.21
EM (c)	12.93	23.70	3.31	13.28	2.89	0.76	0.45	2.64	2.23	0.43	1.18	0.16	1.02	0.15	0.62	1.30
PS (i)	12.57	22.91	3.18	12.72	2.68	0.74	0.45	2.56	2.16	0.42	1.15	0.16	0.99	0.14	0.62	1.17
PS (l)	12.64	23.31	3.14	12.72	2.61	0.76	0.36	2.36	1.95	0.38	1.04	0.14	0.92	0.13	0.63	1.14
BA (c)	10.62	19.68	2.64	10.57	2.18	0.67	0.31	1.91	1.53	0.30	0.83	0.12	0.74	0.11	0.64	1.27
VR (s)	13.91	26.08	3.60	14.97	3.23	0.90	0.50	3.04	2.53	0.48	1.36	0.18	1.17	0.16	0.63	1.34
F (f)	14.14	26.24	3.56	14.51	3.12	0.84	0.50	3.05	2.46	0.49	1.32	0.18	1.17	0.16	0.63	1.29
F (s)	12.85	23.95	3.35	14.47	3.27	0.90	0.57	3.26	2.71	0.52	1.44	0.19	1.22	0.17	0.62	1.29
F (c)	12.68	24.46	3.35	14.00	3.02	0.80	0.56	2.89	2.39	0.45	1.25	0.17	1.08	0.15	0.64	1.27
LM (f)	13.78	26.28	3.58	15.03	3.21	0.92	0.54	3.06	2.50	0.47	1.32	0.18	1.13	0.16	0.64	1.38
LM (c)	13.23	23.97	3.42	14.17	3.20	0.83	0.53	3.11	2.53	0.50	1.38	0.19	1.16	0.16	0.61	1.23
LM (l)	11.90	21.85	2.97	12.06	2.55	0.71	0.42	2.41	1.99	0.39	1.07	0.15	0.94	0.13	0.63	1.35
CH (s)	15.82	30.16	4.11	16.60	3.50	0.98	0.51	3.18	2.55	0.49	1.35	0.18	1.15	0.16	0.64	1.38
CH (c)	16.43	30.80	4.25	16.86	3.48	1.01	0.51	3.28	2.66	0.51	1.40	0.19	1.22	0.18	0.63	1.40
CH (l)	16.94	31.91	4.25	17.01	3.45	0.99	0.45	3.17	2.52	0.49	1.36	0.19	1.19	0.17	0.64	1.41
Average	15.50	28.38	3.88	15.88	3.33	0.89	0.50	3.08	2.56	0.49	1.36	0.19	1.19	0.17	0.63	1.28
Standard deviation	3.72	7.76	0.99	4.04	0.73	0.14	0.08	0.61	0.53	0.10	0.28	0.04	0.26	0.04	0.01	0.08

Anomalies are Ce/Ce* = $3(Ce_N/2(La_N + Nd_N)$ and Eu/Eu* = Eu/Eu* = $Eu_n/[(Sm_n)(Gd_n)]1/2$ subscript $_N$ = normalized values (Taylor and Mc Lennan, 1985).

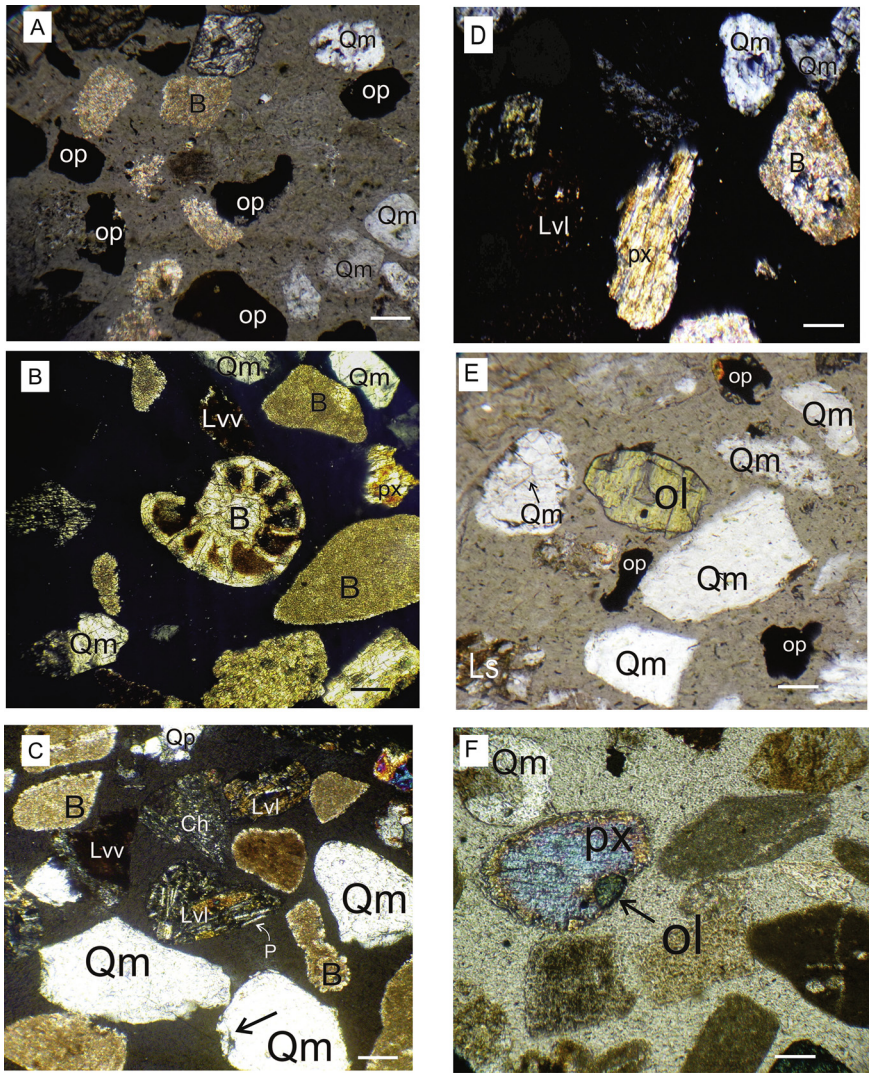

Fig. 5. Photomicrographs of **(A)** monocrystalline quartz (Qm) and opaque minerals (op), sample Le (l); **(B)** monocrystalline quartz (Qm), biogenic fractions (B), pyroxene (px), and volcanic lithics with vitric texture (Lvv), sample Le m (2); **(C)** angular-to-subrounded monocrystalline quartz (Qm) with slight overgrowth (arrow), volcanic lithic with lathwork texture (Lvl) with embedded plagioclase (P), volcanic lithic with vitric textures (Lvv) and chert (Ch), sample PS c (l); **(D)** monocrystalline quartz (Qm), volcanic lithic with lathwork texture (Lvl), pyroxene (px), sample PS c1 **(E)** angular to subrounded monocrystalline quartz with cracks (arrow) (Qm), sedimentary lithic (Ls), free-olivine (ol), opaque minerals (op), sample BA c 1 **(F)** monocrystalline quartz (Qm) and clinopyroxene (px) with embedded olivine crystal (ol) sample VR (s2). Bar scale 500 μm.

index applies to acid, intermediate, and basic rocks. In our study we included the WIP as a measurement of the relative mobility of sodium, potassium, magnesium, and calcium to observe the weathering effect by warm conditions and coastal dynamics. The mean PIA, CIW, and WIP values for the CD and beach sands are 60.44 ± 2.53, 64.51 ± 1.91, and 31.74 ± 4.50, respectively (Figs. 7A–C). In the following section, we discuss some weathering indices in CD sands in arid areas in NW Mexico. In Fig. 7A, we show the weathering values for most of the sand samples grouped near the 70 mark in the A-CN-K. The CIW vs. PIA plot shows a close and inconspicuous variation in the geographical distribution of sands studied in the WGM, where a differentiated subgrouping of sand samples cannot be established (Fig. 7B). The WIP vs. CIA plot shows a poor significance regarding the geographical distribution of the CD and beach sands when visualizing low WIP values compared to the intermediate CIA values (Fig. 7C).

4.7. X-ray diffractograms

The most abundant minerals detected with the difractograms were quartz followed by calcite, clinochlore, ilmenite, andesine, albite, augite, and fayalite. X-ray powder diffraction analysis showed that the southernmost CD and beach sands concentrate albite but they were depleted in ilmenite i.e. samples LM and CH (Figs. 8A–D). Peak maxima for quartz calcite, andesine, and ilmenite were identified for the Istirinchiá site (I s). Main peaks for the Palma Sola site (PS l) were observed for quartz, augite, ilmenite, and calcite. The southern sites show XRD peaks of quartz, calcite, and andesine i.e. the La Mancha site (LM l) whereas the peak maxima for the Chachalacas location (CH c) were identified for quartz, calcite, chlorite, and albite. The modal analysis and the XRD results are in concordance with the mineralogical framework of the CD and beach sands.

5. Discussion

5.1. Grain size and sorting

Medium-to-fine moderately-well-sorted sands were observed in this study. Similar granulometry patterns from coastal dune sands distributed globally have been previously reported (Ahlbrandt, 1979; Kasper-Zubillaga et al., 2007). The fine-grained and well-sorted sands are controlled by the presence of heavy minerals and fine-grained volcanic lithics concentrated in fine fractions (< 2.0 ϕ), while the medium-to-fine, moderately-sorted sands are most likely controlled by the large-size quartz, volcanic lithics, and biogenic fractions deposited in the foreshore of the beach and the stoss face, the crest, and the lee face of the CD sands. Variations in sand size values have been documented elsewhere (Abuodha, 2003; Kasper-Zubillaga and Zolezzi-Ruiz, 2007; Carranza-Edwards et al., 2018). No significant changes in grain size nor in sorting parameters were observed throughout the CD and beach sand sampling from the northern locality of Istirinchiá to the

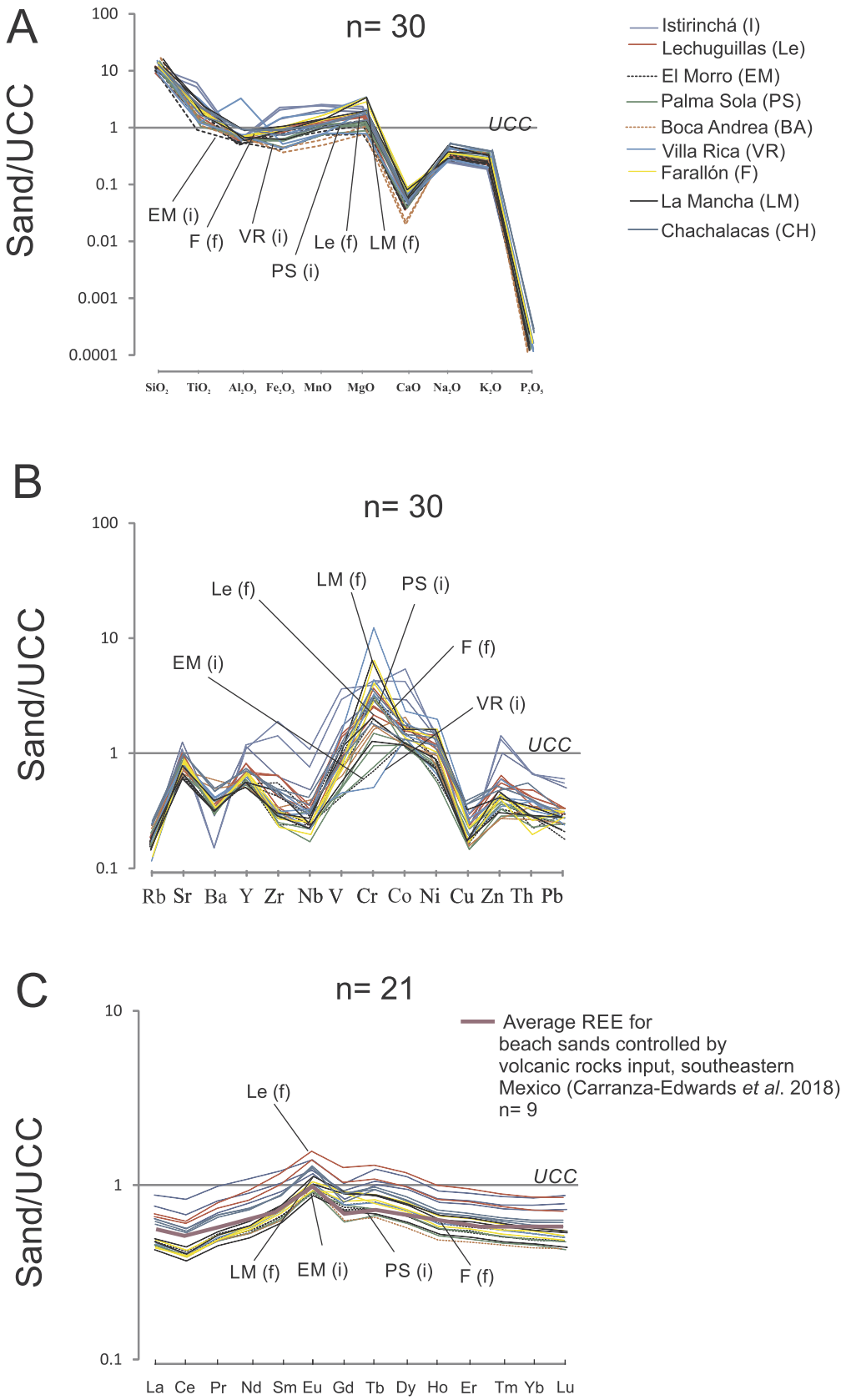

Fig. 6. UCC-normalized **(A)** major; **(B)** trace; and **(C)** rare earth element data (Taylor and Mc Lennan, 1985).

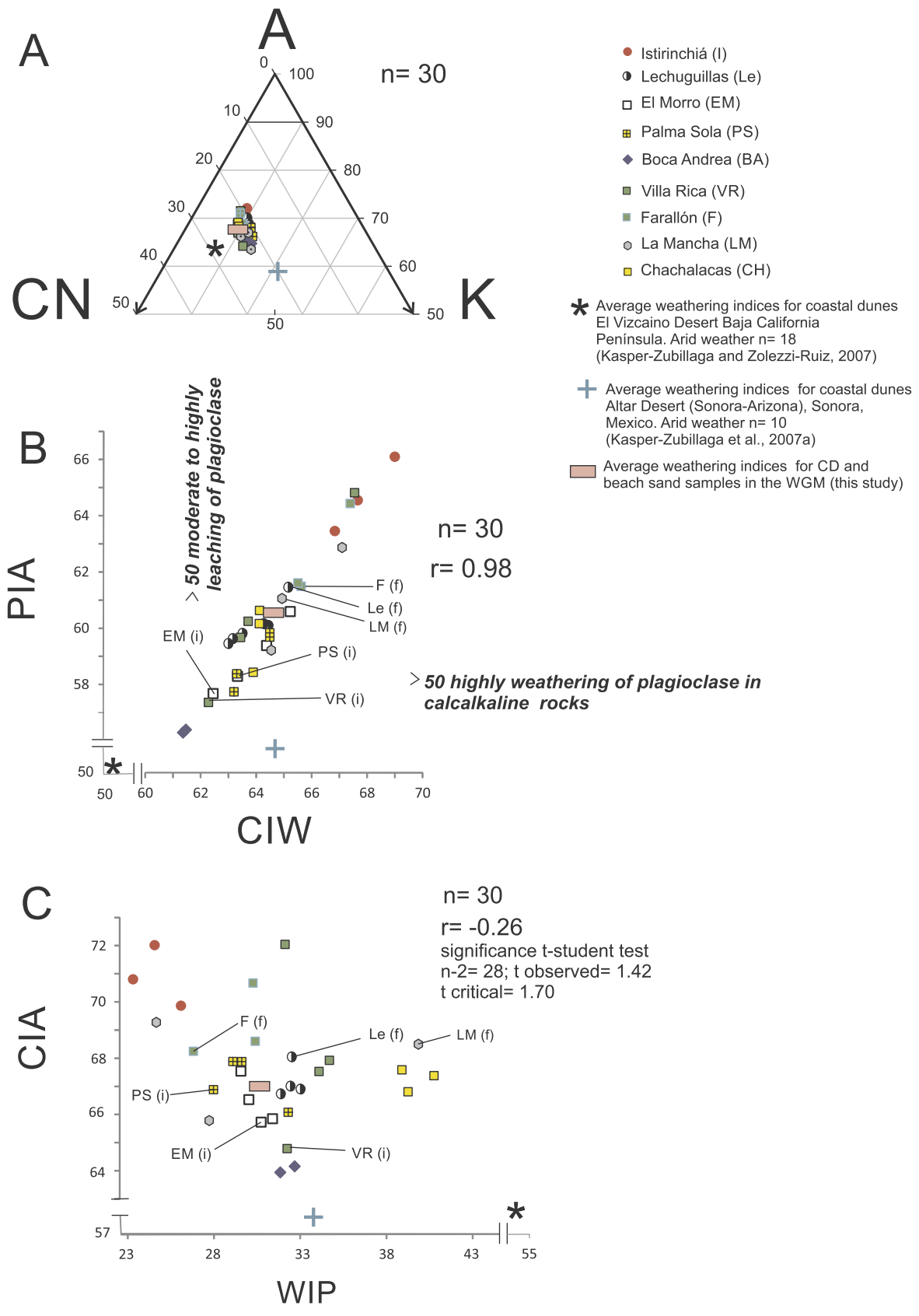

Fig. 7. (A) A-CN-K ternary diagram where A = aluminum, CN = calcium, sodium, and K = potassium; **(B)** CIW vs. PIA plot; **(C)** WIP vs. CIA. Scale break is shown in Figs. 7B and 7C.

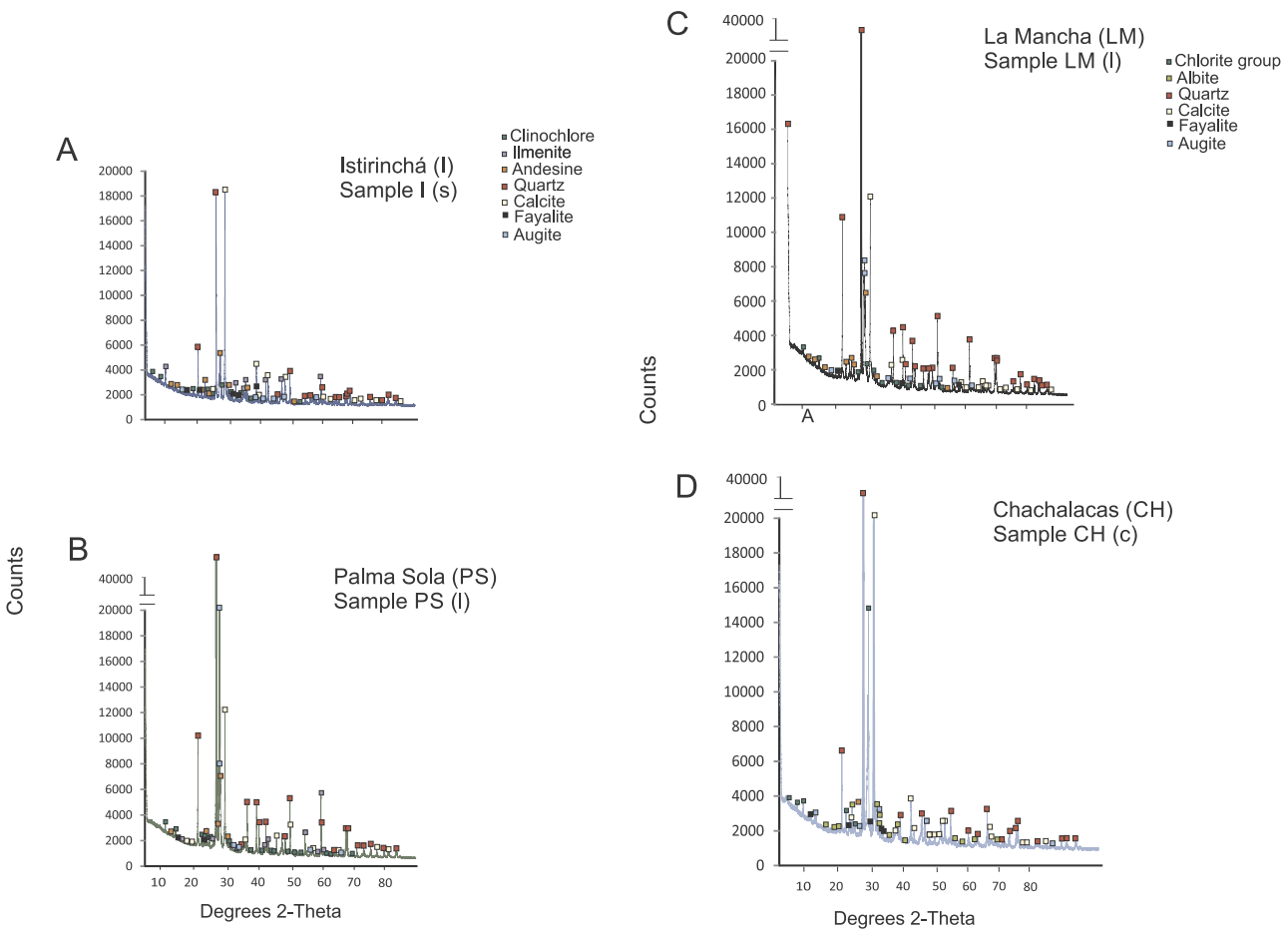

Fig. 8. X-ray diffractograms of samples **(A)** I (s);**(B)** PS (l); **(C)** LM (l); **(D)** CH (c).

Chachalacas site (Table 1). Wind selectiveness may participate in the control of homogenous granulometry considering the whole bulk composition of the sands.

5.2. Modal analysis in the CD and beach sands of the WGM

The CD and beach sands are quartzolithic i.e. $Q_{63}F_1L_{36}$ and $Q_{56}F_1L_{43}$ respectively (Dickinson and Gehrels, 2000). Some studies performed in beach sands in humid and temperate climates have evaluated the role of volcanic rocks as part of the weathering conditions of modern sands (Marsaglia, 1993; Critelli et al., 1997; Morrone et al., 2016). Even with the proximity of the TMVB to the beach sites studied, monocrystalline quartz is one of the main mineralogical frameworks of the whole bulk composition of the CD and beach sand samples. Corroded angular to sub-rounded monocrystalline quartz with some overgrowths was concentrated in the CD and beach sands (Figs. 5B, C). This suggests that vigorous coastal dynamics enhance quartz enrichment input when recycling of monocrystalline quartz occurs. The presence of alluvial deposits in the WGM coastal plain contributes to the quartz enrichment of recycled sands in geographical settings with sub-humid warm weather such as that of the WGM region (Muhs, 2004; Garzanti et al., 2013a, 2013b). Concentration of monocrystalline quartz in the CD and beach sands is also produced by the disaggregated polycrystalline quartz fractions in coarse-grained sizes (e.g. < 2.0 ϕ) which increase the content of corroded single quartz grains in fine-grained CD and beach sands, as documented elsewhere in high-energy sedimentary environments (Harrel and Blatt, 1978). Concentration of monocrystalline quartz in the CD and beach sands suggests longshore transport i.e. angular and sub-rounded quartz and vigorous high wave energy in the beach areas. These are concentrated in the northern sites where longshore currents with a northwesterly direction transport and deposit Qm to the Istirinchiá, Lechiguillas, and El Morro CD and beach sites (Fig. 4A).

The CD and beach sands in the WGM are depleted in single-crystal Ca-Na plagioclase which is only observed as isolated elongated grains within dominant volcanic lithics with lathwork texture in the whole bulk composition of the CD and beach sands (Fig. 5C). Plagioclase is derived from the denudation of mafic basaltic lavas with calc-alkaline and Na-alkaline lavas emplaced as part of the eastern TMVB (Negendank et al., 1985). Depletion in plagioclase is due to a) high rainfall rates in the area with sub-humid warm weather, and b) mechanical abrasion of plagioclase produced by longshore transport/waves and wind deflation, according to several studies performed in ancient and modern sedimentary environments (Dutta et al., 1993; Nesbitt et al., 1997; Muhs et al., 2003; Carranza-Edwards et al., 2018).

High L concentrations in the CD and beach sands were characterized by the following abundances: Lvl < Lvm < Lvv < Ls. This compositional proportion of volcanic lithics or Lvl + Lvm + Lvv is produced by the denudation of calc-alkaline basalts, andesites, Na-alkaline lavas and most probably rhyolite tuffs. The concentration of volcanic lithics in the CD and beach sands is associated with high-energy coastal dynamics exerted by vigorous wave energy and wind deflation of light minerals i.e. quartz as it is observed in CD and beach sands from Mexico (Carranza-Edwards et al., 2018). The Lvl are preserved due to the longshore currents and probably to wind transport, which produces a high concentration of volcanic lithic i.e. Lvl southwards as it is supported by the trends shown in Fig. 4A i.e. samples from Villa Rica (VR), Farallon (F), La Mancha (LM), and Chachalacas (CH). A lower concentration of Ls composed of sandstone and chert fractions derived from the alluvial deposits concentrates in the CD and beach sands. Most of

the calc-alkaline type basalts concentrate towards the Lvl pole due to the dominant mafic basalt fragments in the CD and beach sand samples (Fig. 4B). Our interpretation relies only on the high concentration of the samples towards the Lvl poles which agrees with the high energy environment and dynamic longshore currents.

5.3. Heavy minerals in the CD and beach sands of the WGM

Most of the concentration of opaque minerals is derived from calc-alkaline basalts and it is located in the northern area of the WGM. Opaque minerals in the CD and beach sands are also concentrated near the Sierra Madre Oriental in northeastern Mexico. In our study, ilmenite is identified as the major component of opaque minerals (Fig. 8 a) < 50% TiO_2 mark and also corresponds to the composition of basalts from India (Nawesgara-Rao et al., 2012). Ilmenite lag deposits are probably a mixture of coastal marine and wind processes with vigorous wave energy and longshore surficial current velocities of 8.0 cm s^{-1}, close to the northern CD and beach sites (i.e. the I, Le, and EM sites). In contrast, removal of light fractions such as quartz and biogenic detritus from the CD and beach sands reduces the ilmenite lag deposits at the southern sites (i.e. Palma Sola to Chachalacas) (Fig. 4C) (Fernández-Eguiarte et al., 1992; Abuodha, 2003). This last statement is evidenced by (a) the *in situ* wind speed measurements together with the seasonally average winds observed in charts (Pérez-Villegas, 1990) compiled for all beach localities, and (b) wind deflation seems to be stronger at the northern beach sites (Table 1). Clinopyroxene (augite) is present as phenocrysts concentrated homogeneously in the whole bulk composition of the CD and beach sands. Olivine (fayalite) coexists as part of the clinopyroxenitic phenocrysts, suggesting a possible influence of Na-alkaline lava and/or rhyolitic origin (Grebennikov and Maksimov, 2006) (Fig. 5d). Depletion of single crystals of fayalite was observed due to vigorous coastal dynamics and also to the sub-humid warm weather in the region (Meysman and Montserrat, 2017). Grouping of HM data in the ternary diagram (Fig. 4C) supports the major concentration of op minerals in the CD and beach sands due to vigorous long shore currents, waves and wind deflation. Moderately-well-sorted sediment may also be responsible, evidenced by the ilmenite grain lag deposits at the northern beaches (Istirinchia, Lechuguillas, and El Morro sites) along with periods of high erosion of light minerals and deposition of heavy minerals on the beach as a result of vigorous coastal dynamic processes (Gujar et al., 2010; Sengupta and Van Gosen, 2016).

5.4. Major and trace elements in the CD and beach sands of the WGM

High concentrations in the CD and beach sands of SiO_2, TiO_2, Fe_2O_3, MnO, and MgO above the UCC are a result of volcanic rocks of calc-alkaline to alkaline composition in the form of quartz (SiO_2), ilmenite ($FeTiO_3$), augite (Ca,Na)(Mg,Fe,Al,Ti)$(Si,Al)_2O_6$, and fayalite (Fe_2SiO_4). MnO is derived from basaltic rocks (Weber et al., 2008) while a decrease in CaO concentration in terrigenous fractions is associated with depletion of single-crystal of plagioclase in the whole bulk composition of the sands. Significant correlations between Qm vs. SiO_2, HM vs. TiO_2, HM vs. Fe_2O_3, px vs. Mg support a high concentration of particular major elements and their mineral associations, i.e. monocrystalline quartz-silica, opaque-titanium-iron, and pyroxene-magnesium. Allochthonous shells i.e. mollusks and foraminifera are composed of Ca-calcite detected by the X-ray diffraction spectra which is typical in tropical seas (25 to 30 °C) (Figs. 5A, Figure 6A, Figure 8A–D). Highly variable LOI values of are probably related to the water content in siliciclastic fractions, i.e. plagioclase and carbonate content in the CD and beach sands. However, the significant correlation between LOI and CaO is probably due to the high biogenic content in the CD and beach sands.

5.5. Trace elements in the CD and beach sands of the WGM

The Co abundance is linked to the concentration of Lvl, Lvm, and Lvv in basalts and andesites (Marsaglia et al., 2016; Morrone et al., 2016). Concentrations of Ni are associated with the presence of ferromagnesian minerals, detrital primary Fe and Mn oxides, and most likely with the olivine content in Lvl fractions (Wedepohl, 1969; Lynn et al., 2017). Trace elements are in agreement with the modal, major element, and X-ray diffraction analyses performed.

5.6. REEs in the CD and beach sands of the WGM

Homogeneous flat-type trends without any enrichment of heavy rare earth elements (HREE, Gd-Lu) compared to light rare earth elements (LREE, La-Sm) were observed in the WGM sands. These patterns indicate a volcanic source for the CD and beach sands similar to the REE concentration trends observed in mafic volcanic rocks, neovolcanic rocks, basalt lavas, and tuffs of mild alkaline character (Shimokawa and Masuda, 1972; O'Nions et al., 1973). Lavas and/or andesites with phenocrystals of plagioclase contain positive Eu anomalies (Eu/Eu* of up to 1.2) (Arth, 1981). However, during transport from the rock source to the coastal plain, the labile minerals such as plagioclase are lost, while the positive Eu/Eu* values only reflect the remaining plagioclase crystal embedded in the volcanic lithic fractions (Fig. 5C). The results of the normalized REE diagram for the CD and beach sands is < 1.0 from the UCC line, suggesting depletion and fractionation of REEs during weathering and aeolian and marine transport. The REE patterns of the CD and beach sands are similar to those observed in SE Mexico beach sands controlled by volcanic rock sources (Carranza-Edwards et al., 2018) (Fig. 6C). The slightly negative Ce anomalies may be related to the nature of basalts and a possible but reduced influence of rhyolite tuffs in the sand composition (Wedepohl, 1969).

5.7. Provenance and weathering rates in the CD and beach sands

The CIA, PIA, CIW, and WIP estimations showed high values, indicating high depletion of singe-crystal plagioclase and low concentrations of Ca, Na, and K during sand recycling caused by the vigorous coastal dynamics and sub-humid warm conditions in the WGM. We observed that the CD and beach sand samples are grouped in the CIA diagram described as intermediate weathering, regardless of the geographical location. This indicates that the local climate exerts a major control over the weathering rates of the samples regardless of the heterogeneity of the parent rock near the study area, i.e. calc-alkaline andesites, andesites-dacites, basalts, volcanic tuffs, and basaltic breccias. This is also supported by the concentration/depletion of the existing minerals. For instance, major compositional fractions such as Qm are recycled mineral fractions, while P are depleted due to warm humid conditions and vigorous costal dynamics. Subordinate concentration/depletion of fractions such as Lvl, Lvm, Lvv, Ls, and semi unstable and unstable ol, px, a and op depend on coastal dynamic transport and warm climate conditions (Figs. 4–7).

Undifferentiated groupings of CD and beach sands are observed in the CIW vs. PIA plot suggesting that climate and recycling/depletion of mineral fractions by vigorous costal dynamics produce relatively homogeneous intermediate weathering rates along the coast (Fig. 7B). The WIP and CIA plot reported in an area controlled by volcanic provenance does not support uniformity in the weathering rates related specifically to the geographical distribution of the CD and beach sands. This suggests that highly recycled detrital mineral fractions in the sands in a predominantly warm sub-humid climate produce plagioclase depletion and quartz enrichment, mainly at the Istirinchia site (Fig. 4A and C).

The average value of the CIA/WIP ratio suggests intermediate weathering conditions of recycled coastal sands in the CD and beach sands. We compared our results to those observed in sedimentary basins in central Africa where warm humid conditions have experienced intermediate to intense weathering rates markedly controlled by the quartz dilution effect (Garzanti et al., 2013a, 2013b).

In addition, when we compared sands from the WGM to other regions with a dry and template climate such as the El Vizcaino and Altar deserts in NW Mexico, the CIA values for CD sands were 65.68 ± 1.54 and 58.53 ± 2.06 (Kasper-Zubillaga and Zolezzi-Ruiz, 2007; Kasper Zubillaga et al., 2007). The Vizcaino CD sands showed the following mean values on the chemical weathering indices: PIA = 50.00 ± 5.85, CIW = 52.74 ± 5.77, and WIP = 54.03 ± 2.08. The Altar Desert CD sands had the following mean values for the chemical weathering indices: PIA = 53.29 ± 4.62, CIW = 65.04 ± 4.25, and WIP = 33.88 ± 7.63. The CIA/WIP ratio for the CD and beach sands of the WGM was 2.13 (Garzanti et al., 2013a). Therefore, under dry weather conditions, the CD sands showed lower values for average CIA, PIA, CIW, and WIP estimations compared to the WGM sands (Kasper-Zubillaga and Zolezzi Ruiz, 2007; Kasper-Zubillaga et al., 2007; Muhs, 2017). Our interpretation of the weathering rates in the CD and beach sands is evidenced by (a) the modal analysis in which single-crystal plagioclase is nearly absent in most of the CD and beach sands, (b) the mineralogical assessment of low abundances of single-crystal olivine in the sands, (c) the high and low volcanic lithic and ilmenite content associated with a combination of longshore transport and wind deflation in medium-to-fine-grained sizes concentrated at the PS, VR, LM, and CH localities (Kasper-Zubillaga et al., 2007; Carranza-Edwards et al., 2018), and (d) the decrease in CaO* concentration in the silicate fractions determined by geochemical analyses. Despite the fact that the exhumation of the TMVB exposed near a narrow coastal plain should determine the composition of the CD and beach sands, this study shows that CD and beach sands do not completely reflect the whole composition exerted by the TMVB.

6. Conclusions

The CD and beach sands close to the TMVB are determined by the heterogeneity of several hydrodynamic processes such as wind deflation, longshore currents, and waves, producing medium-to-fine moderately-well-sorted sands. Recycled and highly-corroded monocrystalline quartz and plagioclase as well as olivine depletion as single minerals in the sands suggest a mix of vigorous coastal dynamic mechanisms and warm humid weather prevailing in the coastal area close to the TMVB. Volcanic lithic textures i.e. lathwork, microlithic and vitric are in agreement with the geological framework of the TMBV denudation, which is composed of calc-alkaline lavas, andesites, Na-alkaline lavas, and rhyolite tuffs. Direct relationships between mineralogical and geochemical data explain the high content of silica, titanium, iron, magnesium, biogenic calcium, vanadium, chromium and cobalt with minerals associated with recycled monocrystalline quartz, opaque minerals (ilmenite), clinopyroxene (augite), shell fragments, calc alkaline and alkaline basalts and andesites. The XRD analysis reinforced the mineralogical and modal analyses. Quartz enrichment ($^{>}$ Qm) and dilution effects ($^{<}$ Qm) seem to control the mineralogy in the northern (i.e. less volcanic lithic input) and southern sites (i.e. high volcanic lithic input). Although ilmenite lag deposits in the northern sites reflect extreme hydrodynamic conditions and wind deflation, in contrast, depletion of quartz occurs as a consequence of the removal of light minerals.

Acknowledgments

We wish to thank Rufino Lozano-Santa Cruz, Elizabeth Hernández Álvarez, and Dr. Teresa Pi I-Puig for major, trace, rare earth element, and X-ray diffraction analyses performed at the Instituto de Geología and Geophysics, Universidad Nacional Autónoma de México. We would also like to recognize Patrick Weill for his assistance with the English language. This work was funded through the institutional project "Estudio de Procedencia en Ambientes Sedimentarios Recientes mediante el uso de los Minerales Ligeros y Pesados (Proyecto Interno del Instituto de Ciencias del Mar y Limnología No. 109," Instituto de Ciencias del Mar y Limnología, UNAM.

Appendix A. Supplementary data

Supplementary material related to this article can be found, in the online version, at doi:https://doi.org/10.1016/j.chemer.2018.06.004.

References

Abuodha, J.O.Z., 2003. Grain size distribution and composition of modern dune and beach sediments, Malindi Bay coast, Kenya. J. Afr. Earth Sci. 36, 41–54.
Ahlbrandt, T.S., 1979. Textural parameters of eolian deposits. In: McKee, E.D. (Ed.), A Study of Global Sand Seas. Geological Survey Professional Paper 1052, Washington, D.C, pp. 21–58.
Alappat, L., Joseph, S., Tsukamoto, S., Kaufhold, S., Frechen, M., 2016. Chronology and weathering history of red dunes (Teri Sands) in the southwest coast of Tamil Nadu, India. German J. Geosci. 168, 183–198.
Arth, J.G., 1981. Rare-earth element geochemistry of the island-arc volcanic rocks of Rabaul and Talasea, New Britain. Geol. Soc. Am. Bull. 92, 858–863. https://doi.org/10.1130/0016-7606(1981)92<858:REGOTI>2.0.CO;2.
Blott, S.J., Pye, K., 2001. GRADISTAT: a grain size distribution and statistics package for the analysis of unconsolidated sediments. Earth Surf. Process. Landforms 26, 1237–1248.
Cantagrel, J.M., Robin, C., 1979. K-Ar dating on Eastern Mexican volcanic rocks-relations between the andesitic and the alkaline provinces. J. Volcanol. Geotherm. Res. 5, 99–114.
Carranza-Edwards, A., Kasper-Zubillaga, J.J., Martínez-Serrano, R., Cabrera-Ramírez, M., Rosales-Hoz, L., Alatorre-Mendieta, M.A., Márquez-García, A.Z., Lozano-Santa Cruz, R., 2018. Provenance inferred through modern beach sands from the Gulf of Tehuantepec, Mexico. Geol. J. 1–12. https://doi.org/10.1002/gj.3205.
Critelli, S., Pera, E., Ingersoll Raymond, V., 1997. The effects of source lithology, transport, deposition and sampling scale on the composition of southern California sand. Sedimentology 44, 653–671.
Dickinson, W.R., Gehrels, G.E., 2000. Sandstone petrofacies of detrital zircon samples from Paleozoic and Triassic strata in suspect terranes of northern Nevada and California. In: Soreghan, M.J., Geherls, G.E. (Eds.), Paleozoic and Triassic Paleogeograhy and Tectonics of Western Nevada and Northern California. Geological Society of America Special Paper 347, Bouler Colorado, pp. 151–171.
Dott, R.H., 2003. The importance of eolian abrasion in supermature quartz sandstones and the paradox of weathering on vegetation-eree landscapes. J. Geol. 111, 387–405.
Dutta, P.K., Zhou, Z., dos Santos, P.R., 1993. A theoretical study of mineralogical maturation of eolian sand. In: Johnsson, M.J., Basu, A. (Eds.), Processes Controlling the Composition of Clastic Sediments. Geological Society of America. Special Paper 284, pp. 203–209.
Fedo, C.M., Nesbitt, H.W., Young, G.M., 1995. Unraveling the effects of potassium metasomatism in sedimentary rocks and paleosols, with implications for paleoweathering conditions and provenance. Geology 23, 921–924.
Fernández-Eguiarte, A., Gallegos-García, A., Zavala-Hidalgo, J., 1992. Oceanografía Física (Masas de Agua y Mareas de los Mares Mexicanos) IV.9.1, escala 1: 4000.000, Atlas Nacional de México. Instituto de Geografía, Universidad Nacional Autónoma de México, 1 Chart, Mexio.
Ferrari, L., Orozco-Esquivel, T., Manea, V., Manea, M., 2011. The dynamic history of the Trans-Mexican Volcanic Belt and the Mexico subduction zone. Tectonophysics 522-523, 122–149. https://doi.org/10.1016/j.tecto.2011.09.018.
Fiantis, D., Nelson, M., Shamshuddin, J., Goh, T.B., Van Ranst, E., 2010. Determination of the geochemical weathering indices and trace elements content of new volcanic ash deposits from Mt. Talang (West Sumatra) Indonesia. Eur. Soil Sci. 43, 1477–1485.
Folk, R.L., 1980. Petrology of Sedimentary Rocks. Hemphill Publications, Austin, Texas.
Garzanti, E., Padoan, M., Andò, S., Resentini, A., Vezzoli, G., Lustrino, M., 2013a. Weathering and relative durability of detrital minerals in Equatorial climate: Sand petrology and geochemistry in the East African Rift. J. Geol. 121, 547–580.
Garzanti, E., Vermeesch, P., Andò, S., Vezzoli, G., Valagussa, M., Allen, K., Kadi, K.A., Al-Juboury, A.I.A., 2013b. Provenance and recycling of Arabian desert sand. Earth Sci. Rev. 120, 1–19.
Garzanti, E., Resentini, A., Andò, S., Vezzoli, G., Preira, A., Vermeesch, P., 2015. Physical controls on sand composition and relative durability of detrital minerals during ultra-long distance littoral an aeolian transport (Namibia and southern Angola. Sedimentology 62, 971–996.
Goldberg, k., Humayun, M., 2010. The applicability of the chemical index of alteration as a paleoclimatic indicator : an example from the Permian of the Paraná Basin, Brazil. Palaeogeogr. Palaeoclimatol. Palaeoecol. 293, 175–183.
Gómez-Tuena, A., Orozco-Esquivel, M.T., Ferrari, L., 2007. Igneous petrogenesis of the trans-Mexican volcanic belt. In: In: Alaniz-Álvarez, S.A., Nieto-Samaniego, Á.F. (Eds.), Geology of México: Celebrating the Centenary of the Geological Society of México: Geological Society of America Special Paper 422. pp. 129–181.
Grebennikov, A.V., Maksimov, S.O., 2006. Fayalite rhyolites and a zoned magma chamber of the Paleocene Yakutinskaya volcanic depression in Primorye, Russia. J. Miner. Petrol. Sci. 101, 69–88.
Gujar, A.R., N.V, Ambre, P.G, Mislankar, Iyer, S.D., 2010. Ilmenite, magnetite and chromite beach placers from South Maharashtra, Central West Coast of India. Resour. Geol. 60, 71–86.
Harrel, J., Blatt, H., 1978. Polycrystallinity; Effect on the durability of detrital quartz. J. Sediment. Res. 48, 25–30.
Honda, M., Shimizu, H., 1998. Geochemical, mineralogical and sedimentological studies on the Taklimakan Desert sands. Sedimentology 45, 1125–1143.
Kasper-Zubillaga, J.J., Carranza Edwards, A., Rosales-Hoz, L., 1999. Petrography and

geochemistry of Holocene sands in the western Gulf of Mexico: implications for provenance and tectonic setting. J. Sediment. Res. 69, 1002–1010.
Kasper-Zubillaga, J.J., Zolezzi-Ruíz, H., Carranza-Edwards, A., Girón-García, P., Ortiz-Zamora, G., Palma, M., 2007. Sedimentological, modal analysis and geochemical studies of Desert and coastal dunes, Altar Desert, NW Mexico. Earth Surf. Process. Landforms 32, 489–508.
Kasper-Zubillaga, J.J., Zolezzi-Ruiz, H., 2007. Grain size, mineralogical and geochemical studies of coastal and inland dune sands from the El Vizcaino Desert, B.C. México. Rev. Mex. Cienc. Geol. 24, 423–438.
Kottek, M., Grieser, J., Beck, C., Rudolf, B., Rubel, F., 2006. World Map of the Köppen-Geiger climate classification updated. Meteorol. Z. 15, 259–263.
Lozano, R., Bernal, J.P., 2005. Characterization of a new set of eight geochemical reference materials for XRF major and trace element analysis. Rev. Mex. Cienc. Geol. 22, 329–344.
Lynn, K.J., Shea, T., García, M.O., 2017. Nickel variability in Hawaiian olivine: evaluating the relative contributions from mantle and crustal processes. Am. Mineral. 102, 507–518.
Marsaglia, K.M., 1993. Basaltic island sand provenance. In: Johnsson, M.J., Basu, A. (Eds.), Processes Controlling the Composition of Clastic Sediments. Geological Society of America, Boulder, Colorado, pp. 284.
McLennan, S.M., 1993. Weathering and global denudation. J. Geol. 101, 295–303.
Meysman, F.J.R., Montserrat, F., 2017. Negative CO(2) emissions via enhanced silicate weathering in coastal environments. Biol. Lett. 13, 20160905.
Morrone, C., De Rosa, R., Le Pera, E., Marsaglia, K.M., 2016. Provenance of volcaniclastic beach sand in a magmatic-arc setting: an example from Lipari island (Aeolian archipelago, Tyrrhenian Sea). Geol. Mag. 154, 804–828.
Muhs, D.R., 2017. Evaluation of simple geochemical indicators of aeolian sand provenance: late quaternary dune fields of North America revisited. Quat. Sci. Rev. 171, 260–296.
Muhs, D.R., Reynolds, R.L., Been, J., Skipp, G., 2003. Eolian sand transport pathways in the southwestern United States: importance of the Colorado River and local sources. Quat. Int. 104, 3–18.
Muir, I.D., Tilley, C.E., 1961. Mugearites and Their Place in Alkali Igneous Rock Series. J. Geol. 69, 186–203.
Nawesgara-Rao, P.V., Swaroop, P.C., Karimulla, S., 2012. Mineral chemistry of Pangidi basalt flows from Andhra Pradesh. J. Earth Syst. Sci. 121, 525–536.
Negendank, J., Emmermann, R., Krawczyk, R., Mooser, F., Tobschall, H., Wehrle, D., 1985. Geological and geochemical investigations on the eastern Trans-Mexican Volcanic Belt. Geofãsica Int. 24, 477–575.
Nesbitt, H.W., Young, G.M., 1982. Early Proterozoic climates and plate motions inferred from major element chemistry of lutites. Nature 299, 715.
Nesbitt, H.W., Fedo, C.M., Young, G.M., 1997. Quartz and feldspar stability, steady and non steady state weathering, and petrogenesis of siliciclastic sands and muds. J. Geol. 105, 173–192.
Nonnotte, P., Benoit, M., Le Gall, B., Hémond, C., Rolet, J., Cotten, J., Brunet, P., Makoba, E., 2011. Petrology and geochemistry of alkaline lava series, Kilimanjaro, Tanzania: New constraints on petrogenetic processes. In: Beccaluva, L., Bianchini, G., Wilson, M. (Eds.), Volcanism and Evolution of the African Lithosphere. Geological Society of America.
O'Nions, R.K., Pankhurst, R.J., Fridleifsson, I.B., Jakobsson, S.P., 1973. Strontium isotopes and rare earth elements in basalts from the heimaey and surtsey volcanic eruptions. Nature 243, 213.
Ortiz-Pérez, M.A., Espinosa, R.L.M., 1991. Clasificación geomorfológica de las costas de méxico. Geogr. Desarrollo 2, 2–9.
Parker, A., 1970. An index of weathering for silicate Rocks. Geol. Mag. 107, 501–504.
Pérez-Villegas, G., 1990. Clima: Atlas Nacional De México (Hoja IV.4.2). Instituto de Geografía, Universidad Nacional Autónoma de México.
Price, J.R., Velbel, M.A., 2003. Chemical weathering indices applied to weathering profiles developed on heterogeneous felsic metamorphic parent rocks. Chem. Geol. 202, 397–416.
Sengupta, D., Van Gosen, B.S., 2016. In: In: Verplanck, Philip L., Hitzman, Murray W. (Eds.), Placer-Type Rare Earth Elements Deposits In Reviews in Economic Geology 18. Society of Economic Geologists, Inc., pp. 81–100.
Servicio Geológico Mexicano, 2017. Cartografía Geología De La República Mexicana Formato SHP Escala 1:250,000. C.f.S., escala 1:250,000. .
Shimokawa, T., Masuda, A., 1972. Rare-earths in Icelandic neovolcanic rocks. Contr. Miner. Petrol. 37, 39–46.
Tamayo, J.L., 2013. Geografía Moderna de México. Trillas, México. 390 pages. .
Taylor, S.R., Mc Lennan, S.M., 1985. The Continental Crust, Its Composition and Evolution. Blackwell Scientific. Publication, Oxford.
Trumbull, R.B., Bühn, B., Romer, R.L., Volker, F., 2003. The petrology of Basanite–Tephrite intrusions in the Erongo complex and implications for a plume origin of cretaceous alkaline complexes in Namibia. J. Petrol. 44, 93–112.
Weber, B., Valencia, V.A., Schaaf, P., Pompa-Mera, V., Ruiz, J., 2008. Significance of provenance ages from the chiapas massif complex (Southeastern Mexico): redefining the paleozoic basement of the Maya block and its evolution in a peri-Gondwanan realm. J. Geol. 116, 619–639.
Wedepohl, K.H., 1969. Handbook of Geochemistry. Springer-Verlag, Berlin-Heidelberg-New York 1970.